

Almost Heaven, Galactic Center

star formation in the
wild, wonderful
Brick (G0.253+0.016)

Alyssa Bulatek (she/her)
UF Astronomy PhD Candidate (advised by Adam Ginsburg)

Desmond Jeff, Theo Richardson, Nazar Budaiev, Savannah
Gramze, Taehwa Yoo, Jeremy Darling, Christian Henkel, Karl M.
Menten, the ACES Collaboration, and the MUSTANG Team

Credit: NRAO/AUI/NSF; Adam Ginsburg and
John Bally (Univ of Colorado - Boulder),
Farhad Yusef-Zadeh (Northwestern),
Bolocam Galactic Plane Survey team;
GLIMPSE II team

May 2, 2024
Green Bank Observatory Colloquium

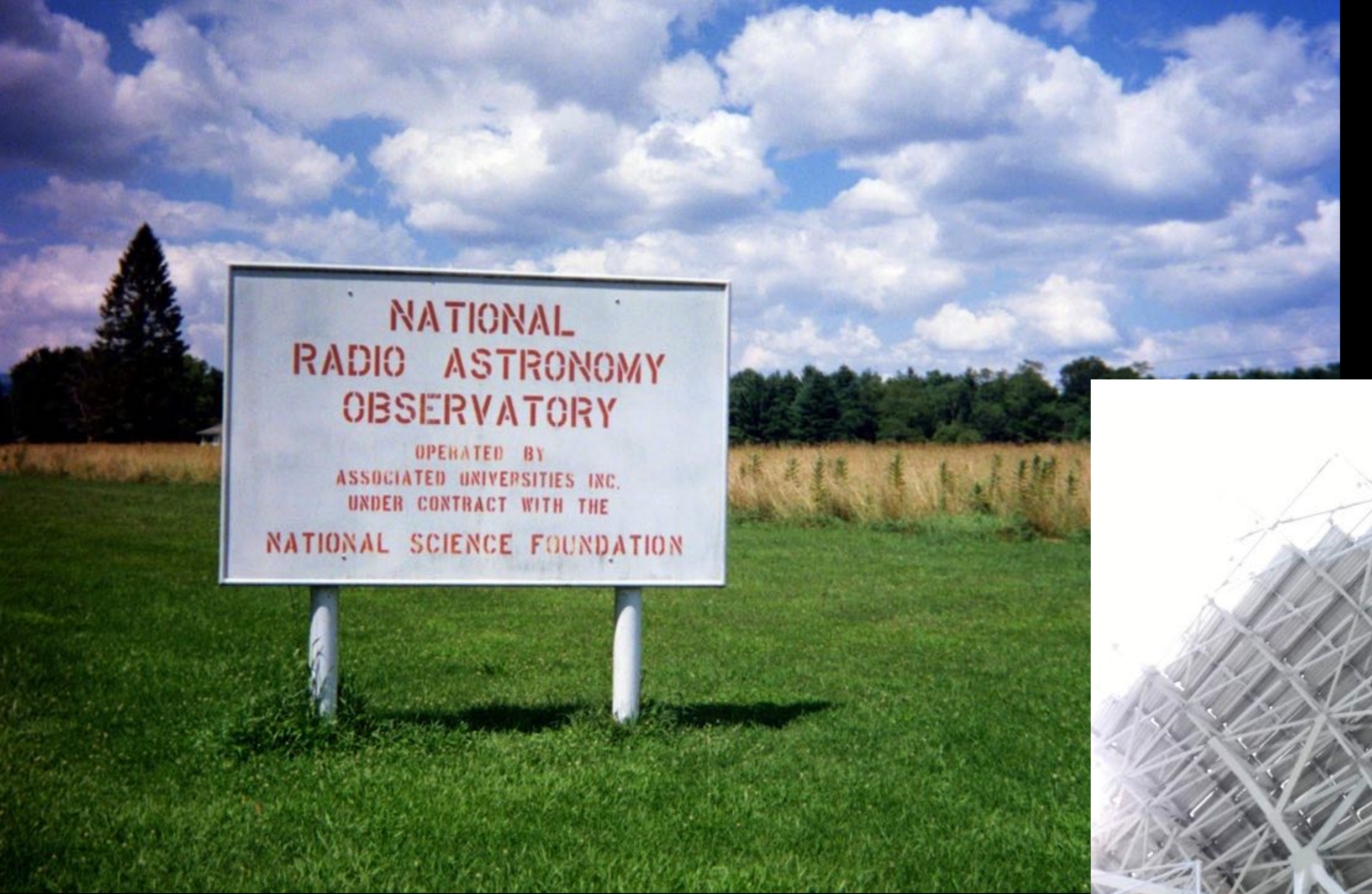
GB and me

Credit: Jill Malusky



Summer 2019







Credit: Don't remember, just got out of a cave

Designing and testing an ultra-wideband receiver for the Green Bank Telescope

Alyssa Bulatek, Macalester College

Advisor: Steve White, Green Bank Observatory

Alyssa Bulatek
Macalester College '20
BA in Physics/Astronomy and
Applied Math/Statistics
abulatek@macalester.edu

January 2020

Abstract

We determined the predicted efficiency and basic circuit characteristics of a new ultra-wideband (UWB; 0.7 to 4.2 GHz) receiver for the Green Bank Telescope (GBT). The UWB receiver has been in development for several years and it represents a movement towards new-age receiver technology for Green Bank Observatory. The design features a quad-ridged, flared feed horn and utilizes a corrugated skirt and a quartz spear to extend the receiver's bandwidth. We find the predicted efficiency of the receiver to be around 60 to 70% at lower frequencies and above 50% at higher frequencies. The S_{11} values for the UWB receiver are better than -10 dB across the entire bandwidth, and performance is only predicted to degrade slightly at 2.8 GHz with the inclusion of a waveguide window. The UWB receiver will be used by the North American Nanohertz Observatory for Gravitational Waves (NANOGrav) to perform pulsar timing experiments using the GBT with greater sensitivity than before. Secondary science drivers for the receiver include the detection of broadband fast radio bursts and other radio transients as well as the study of radio recombination lines.

Motivation

Pulsars are radio-bright, rapidly rotating neutron stars. NANOGrav's mission is to time the rotation of pulsars and detect gravitational waves using variations in their rotational periods. Radio signals from pulsars are subject to frequency-dependent dispersion on their path to the Earth.

Thus, pulsars must be observed using a wide range of radio frequencies to accurately measure their periods. The GBT currently uses its 800 MHz and L-band receivers at different times to observe a single pulsar, which reduces timing accuracy. The sensitivity of pulsar timing observations for the GBT can be improved by a new receiver that can perform wide-band pulsar observations simultaneously.

Specifications

- Frequency range: **0.7 – 4.2 GHz**
→ Bandwidth: **3.5 GHz (6:1)**
- Dimensions: **1.5 m × 1 m**
- Four symmetrically-spaced ridges lower the cutoff frequency of the dominant mode in the horn.
- To reduce spillover at lower frequencies, a **corrugated skirt** encircles the receiver's aperture.
- In the throat, a **dielectric spear** reduces under-illumination at high frequencies.
- A quartz fabric **window** will allow radiation into the receiver.
- Designed in CST Microwave Studio by Steve White.

References

- Beukman, T. S., Meyer, P., Ivashina, M. V., et al. 2016, *ITAP*, 64, 1615
Collin, R. 1984, *ITAP*, 32, 997
Condon, J. J., & Ransom, S. M. 2016, *Essential Radio Astronomy* (Princeton, NJ: PUP)
Kildal, P.-S. 1985, *ITAP*, 33, 903
Lorimer, D. R., & Kramer, M. 2005, *Handbook of Pulsar Astronomy* (Cambridge, UK: CUP)
Ludwig, A. C. 1965, *Space Programs Summary* 37-26, vol. IV, 200-208
Simon, R. J. 2005, *NRAO Electronics Division Internal Report* 315

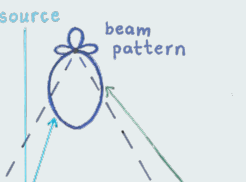
Results

Efficiencies

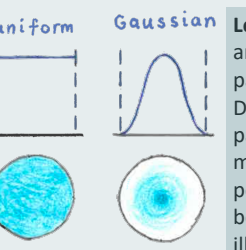
The total **feed efficiency** (e_{tot}) of an antenna is the proportion of the radiation incident on the telescope which gets received and recorded. e_{tot} depends on the shape of the receiver's radiation pattern, which depends on the receiving frequency. The feed efficiency can be divided into **sub-efficiencies** due to spillover (e_{sp}), inefficient dish illumination (e_{ill}), phase errors (e_{ph}), and cross-polarization (e_{xp}). The **balance** between spillover and illumination is the primary predictor of the receiver's efficiency. e_{tot} is the product of its sub-efficiencies:

$$e_{tot} = e_{sp} \cdot e_{ill} \cdot e_{ph} \cdot e_{xp}$$

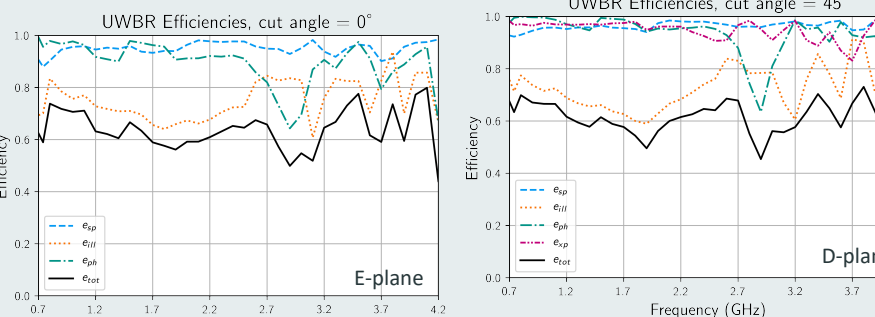
The resulting total feed efficiency will be between zero and one. The design goal for the UWB receiver was to achieve e_{tot} between 60 and 70% at the lower end of the frequency range and above 50% at higher frequencies. We calculated each sub-efficiency as a function of frequency given far-field radiation patterns from our CST model. Since radiation patterns are three dimensional, we sliced through them at three standard azimuthal angles to calculate e_{tot} . Our design goals mentioned above are close to being achieved across the entire frequency band for all cut angles, as can be seen in the efficiency plots below.



Above: a depiction of how both source and spillover radiation reach a receiver.



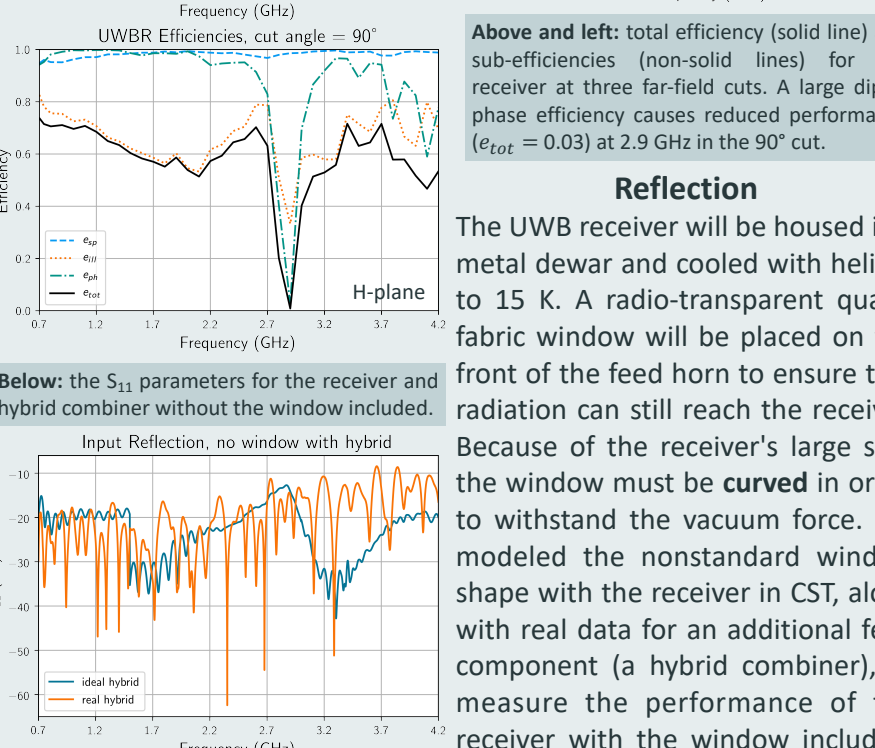
Left: a drawing of uniform and Gaussian illumination patterns in 1D and 2D. Designing a radiation pattern to perfectly edge-match its reflector is not possible, so the balance between spillover and illumination is important.



Above and left: total efficiency (solid line) and sub-efficiencies (non-solid lines) for the receiver at three far-field cuts. A large dip in phase efficiency causes reduced performance ($e_{tot} = 0.03$) at 2.9 GHz in the 90° cut.

Reflection

The UWB receiver will be housed in a metal dewar and cooled with helium to 15 K. A radio-transparent quartz fabric window will be placed on the front of the feed horn to ensure that radiation can still reach the receiver. Because of the receiver's large size, the window must be **curved** in order to withstand the vacuum force. We modeled the nonstandard window shape with the receiver in CST, along with real data for an additional feed component (a hybrid combiner), to measure the performance of the receiver with the window included.



Acknowledgements

I would like to thank my advisor, Steve White, for his support and guidance on this project. I would also like to thank Bob Simon, Ryan Lynch, Sivasankaran Srikanth (NRAO CDL), Lisa Locke (NASA JPL), and Nathaniel Sizemore for their valuable input on this project. Additionally, I would like to thank the other scientists, engineers, staff members, and summer students at GBO who made my summer an extremely positive experience. This project was funded by the NSF through the REU program at the Green Bank Observatory. The Green Bank Observatory is a facility of the National Science Foundation operated under cooperative agreement by Associated Universities, Inc.

Results (continued)

Treating the receiver as a transmitter, the **S_{11} parameter** for the window represents the fractional amount of signal reflected back from the window. Our design goal for the S_{11} parameter of the feed with a window included was -10 dB or better. A signal that is 10 dB lower than another signal is one-tenth as powerful. The S_{11} parameter across the bandwidth is not degraded significantly when the window is included with the receiver in the model.

Left: the S_{11} parameters for the receiver and hybrid combiner with the window included. Note the near compliance with the design guideline (less than -10 dB).

Since the window must withstand large forces due to vacuum pressure in the dewar, **destructive tests** must be performed. The latest prototype burst at 66 psi, as expected.



Above: (a) shows the 8" diameter prototype. (b) shows the prototype in the pressure vessel. (c) shows the prototype after bursting. (d) shows a 40" diameter spun dome which will be the mold for the final window. Images courtesy of Bob Simon.

Conclusions

- The ultra-wideband receiver **meets its efficiency design goals** in its "frozen" design state.
- The waveguide window has **only a minor effect** on the circuit properties of the feed horn.

Future Work

Current Project Status

- ✓ All **mechanical drawings** for the feed and its components are complete. Fixtures have been fabricated for holding the components in place while they are machined.
- ❑ The ridges will be the first components to be fabricated.
 - Mechanical drawings have been sent to Art Symmes at NRAO Charlottesville for **thermal modeling** of the feed and the dewar that will house it.
- ✗ The software development for the UWB receiver **backend** is also progressing. The control software for the receiver will be an extension of the existing VEGAS backend. Prototyping is beginning on the manager for the receiver and physical upgrades to the server room are in progress.

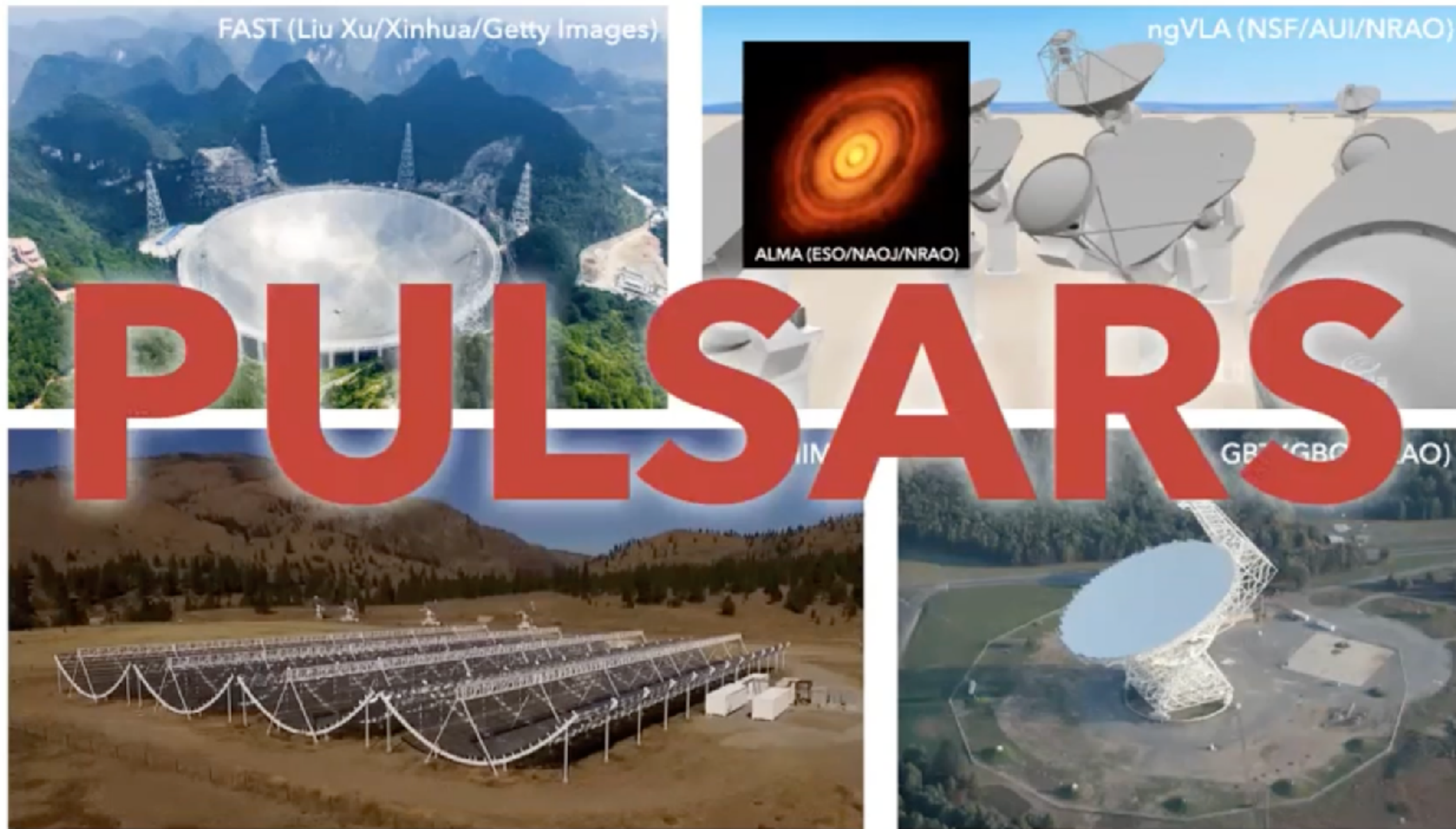
Modal-Based Receiver Design

- Even though the effect of the reduced efficiency at 2.9 GHz can be mitigated, its origin still sparks curiosity. All the undesirable radiation pattern characteristics that stem from the UWB receiver's geometry are most likely related to the **imbalance of higher-order mode excitation** in the feed horn.
- Beukman et al. (2016) present a design technique focused on understanding the modal content of the feed horn to determine the ideal parameters for the horn geometry without brute-force optimization. As my senior honors thesis, I will determine the modal makeup of the radiation patterns for the UWB receiver to inform GBO's receiver design process.





THE FUTURE OF RADIO ASTRONOMY



April 2020

Star formation in an extreme environment

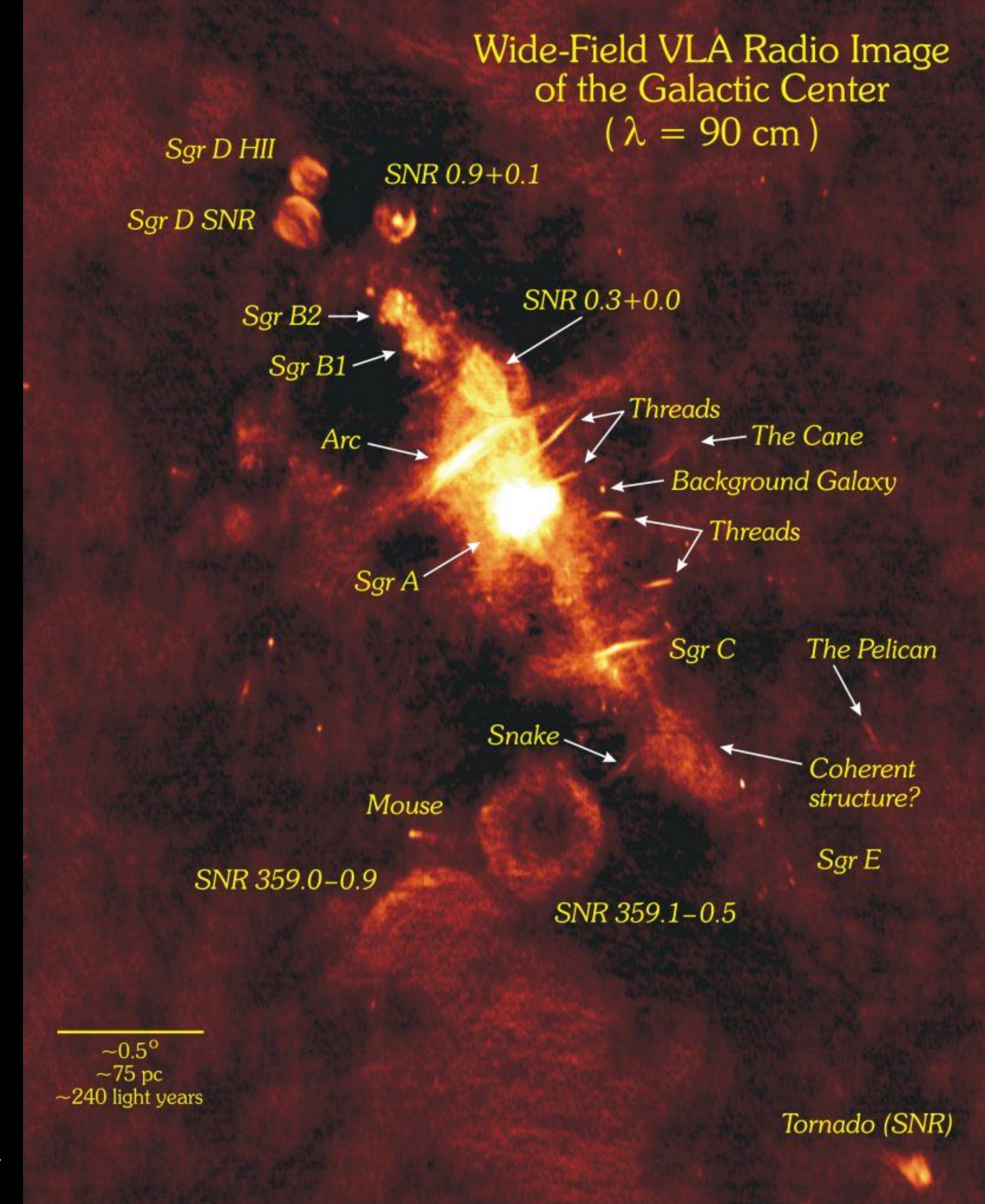
Quick note



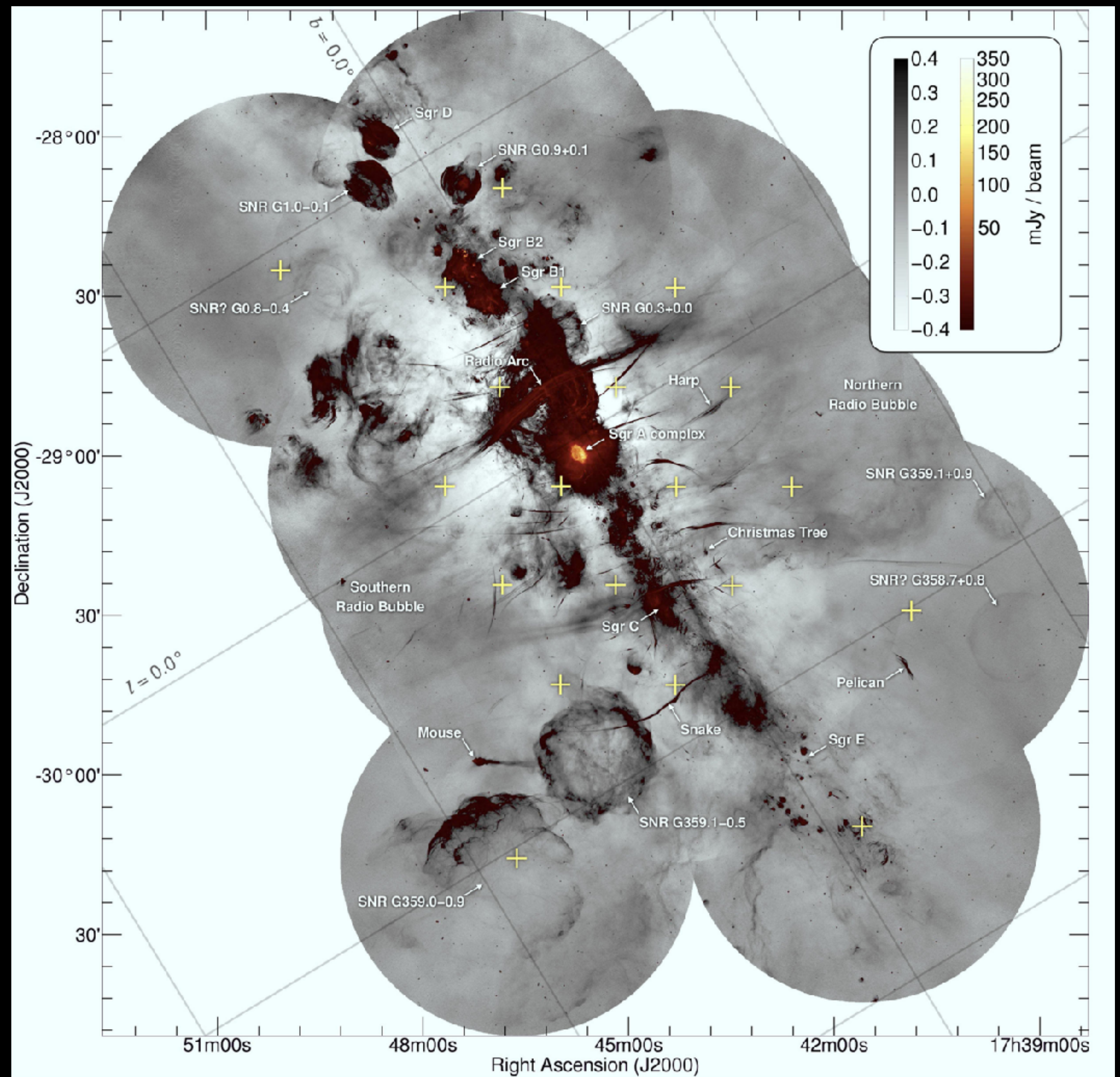
I use the following terms interchangeably:

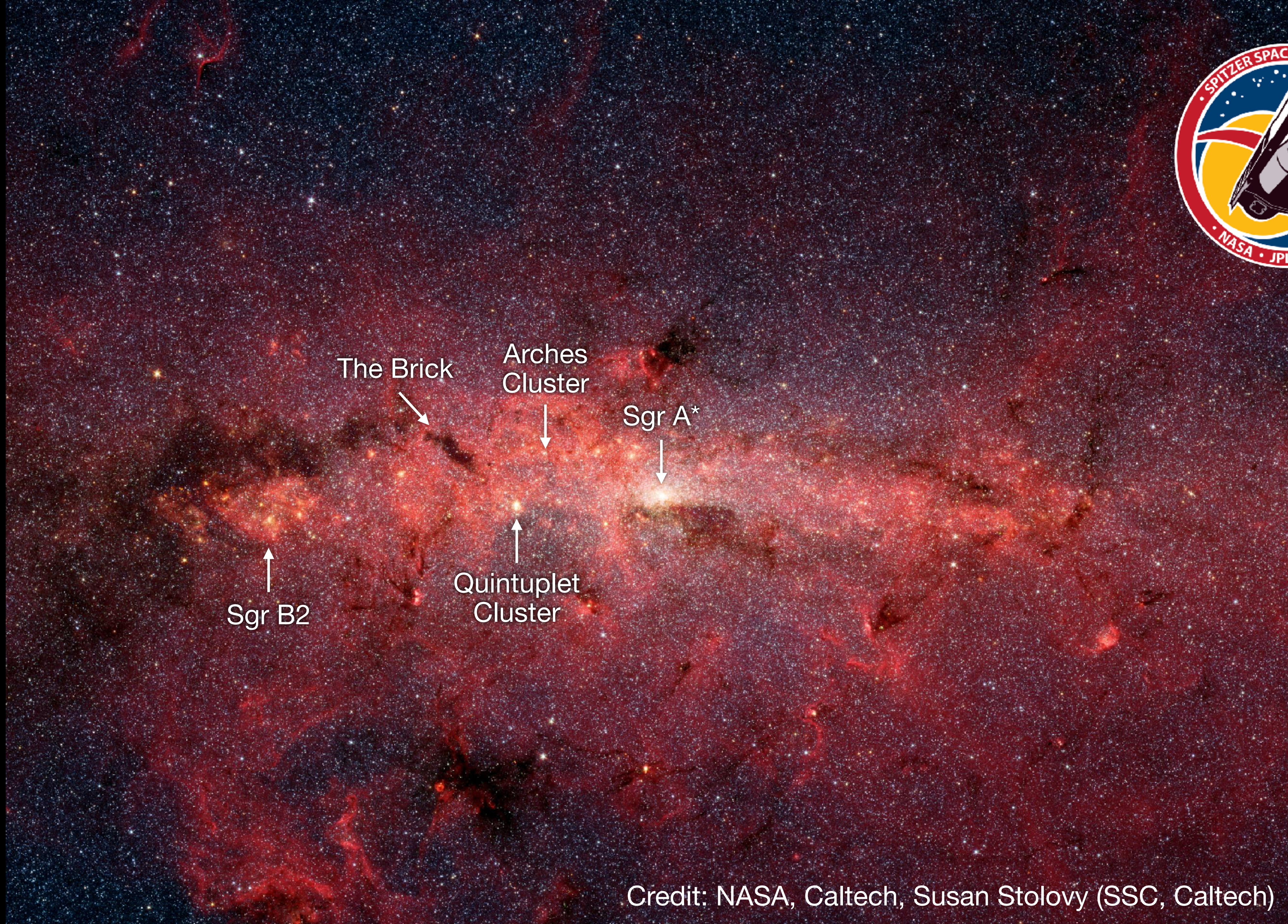
- **Galactic Center** = GC: the inner part of the Milky Way
- **Central Molecular Zone** = CMZ: molecular material within $R_{Gal} \approx X00$ pc

Wide-Field VLA Radio Image
of the Galactic Center
($\lambda = 90$ cm)



Credit: N.E. Kassim, Naval
Research Laboratory



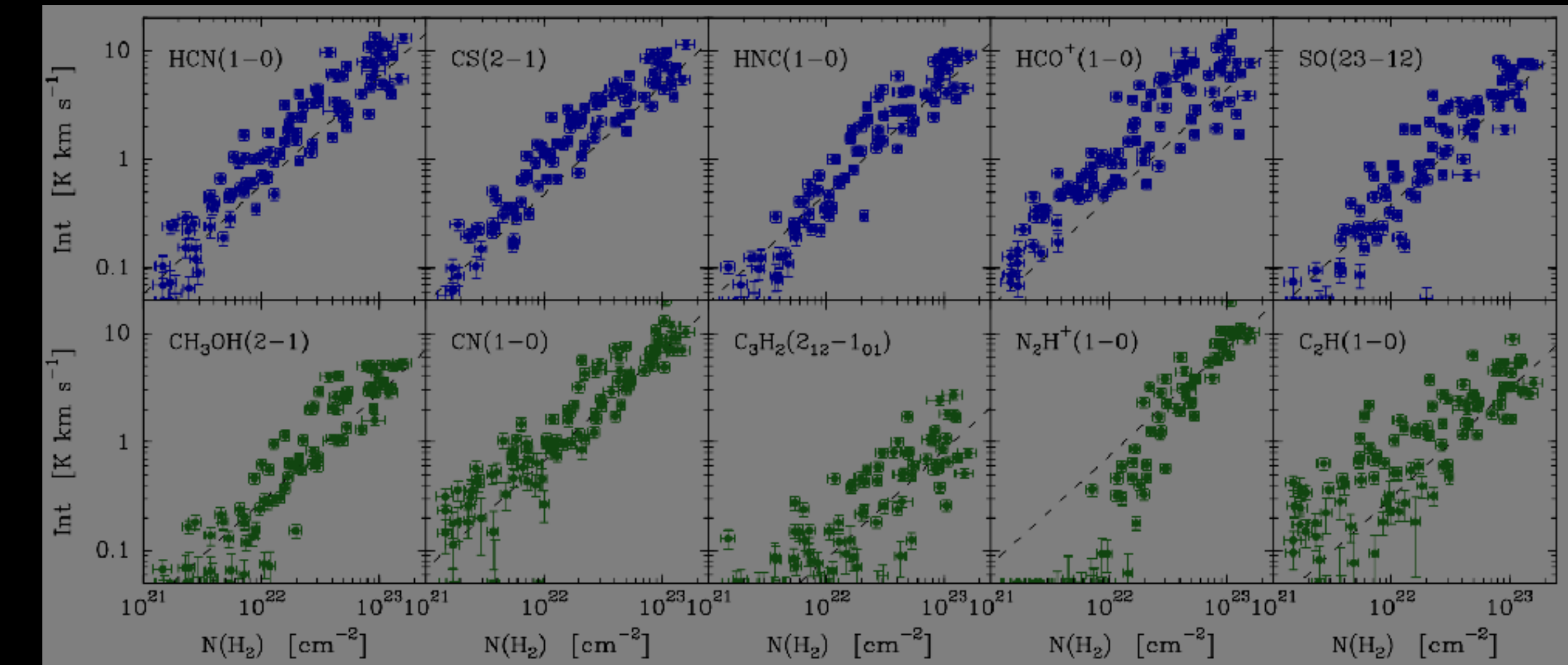
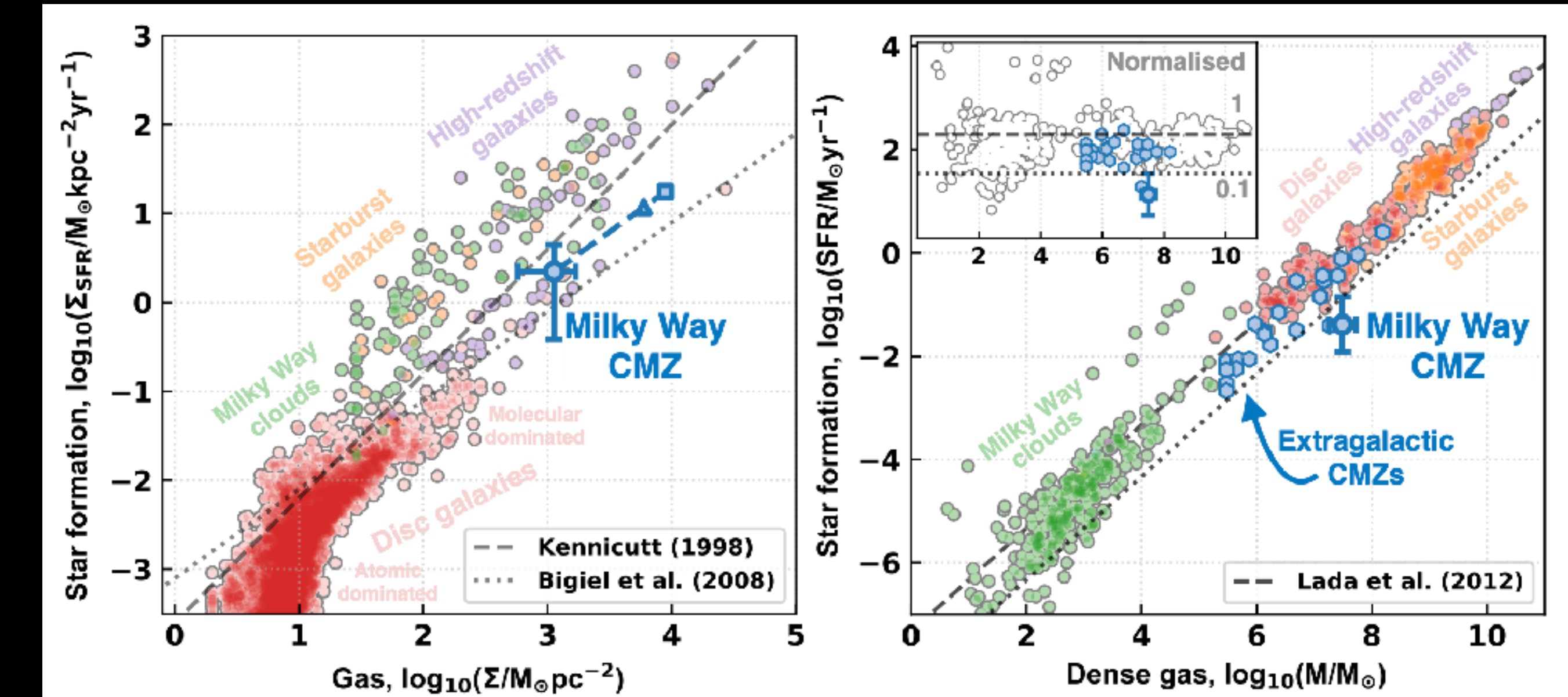


Credit: NASA, Caltech, Susan Stolovy (SSC, Caltech)

Open questions in Galactic Center star formation

- How do stars form in the Galactic Center?
- Why is star formation in the GC different than in the Galactic disk?
- What are the initial conditions for SF in the GC?
- What role do chemistry, turbulence, and gas kinematics play in GC SF?
- Why is The Brick forming so few stars?

Henshaw+2023



Tafalla+2021

CMZ Quantities

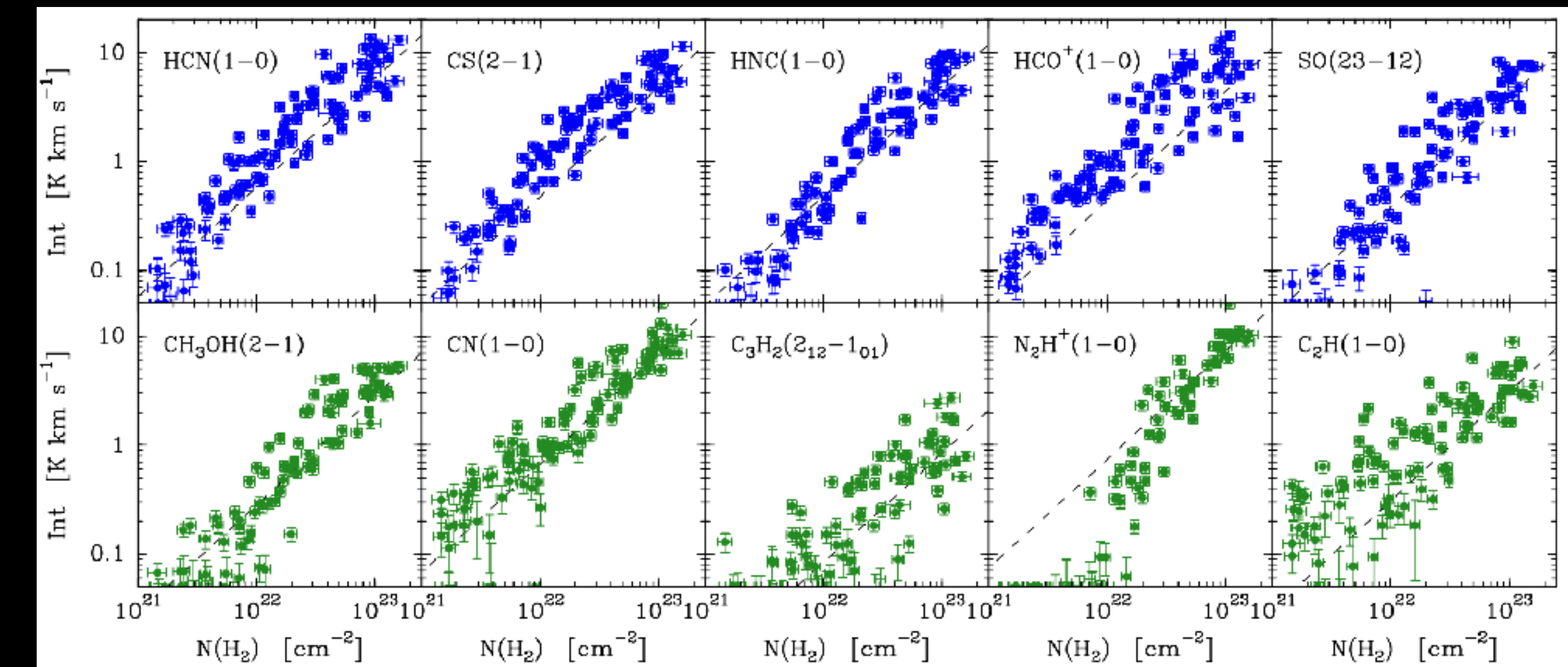
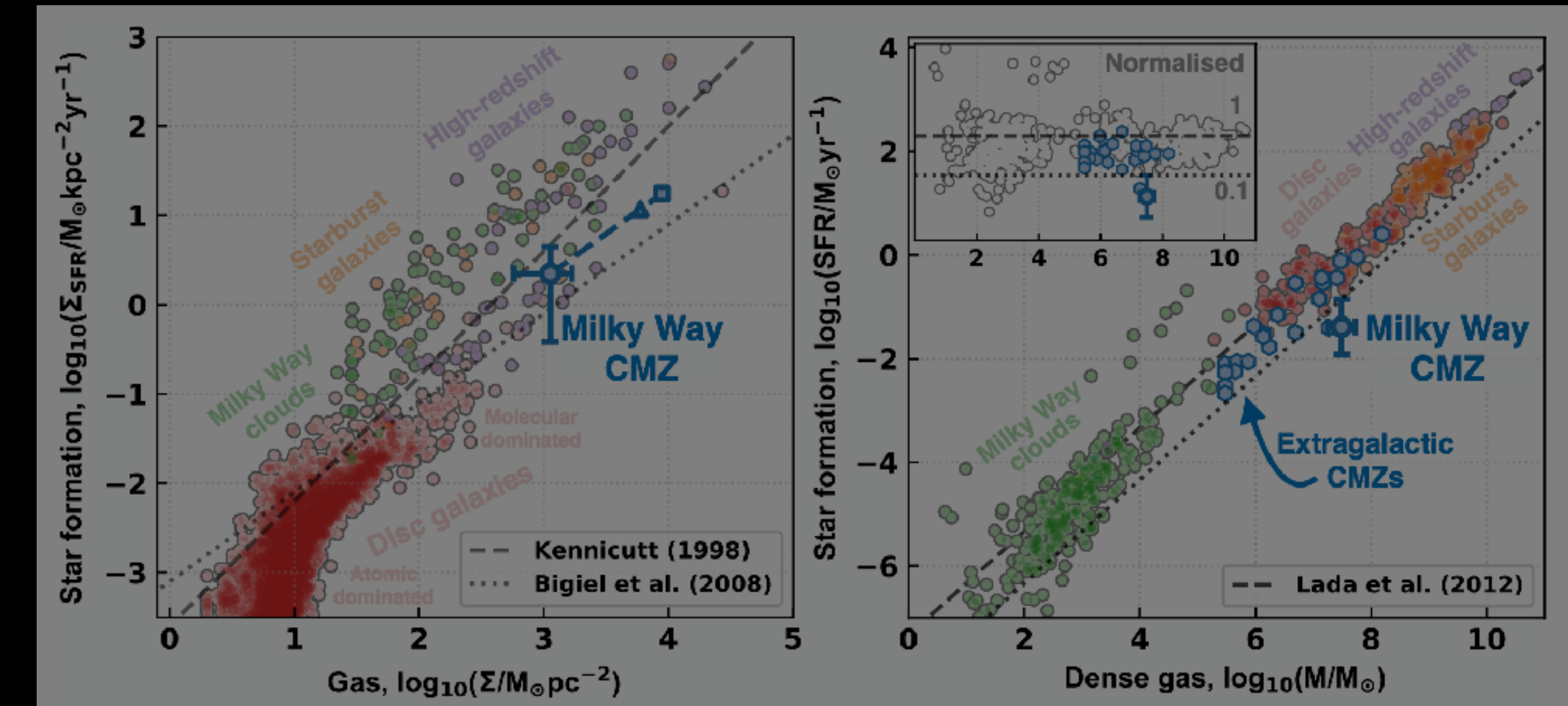
Henshaw+2023

Physical Quantity	CMZ	Solar Neighbourhood	Extragalactic CMZs	$z \sim 2$
Distance [kpc] ^(a)	8.2	0.1 - 0.5	3500 - 20000	$\sim 10^6$ ($z \sim 2$)
SFR [$M_{\odot} \text{yr}^{-1}$] ^(b)	0.07 (0.012-0.14)	0.002	0.001-0.08	1-100
Σ_{gas} [$\log_{10}(M_{\odot} \text{pc}^{-2})$] ^(c)	3.1 (2.8-3.2)	1.5	0.6-3	1.5-3.5
Σ_{SFR} [$\log_{10}(M_{\odot} \text{yr}^{-1} \text{kpc}^{-2})$] ^(d)	0.3 (-0.4-0.6)	-2.5	-3-0	-1.5-1.5
Σ_{*} [$\log_{10}(M_{\odot} \text{pc}^{-2})$] ^(e)	3.9	1.5	3.4-3.9	1-4
t_{dep} [Gyr] ^(f)	0.5 (0.4-1.5)	1	0.3-2.6	0.2-1
t_{dyn} [Myr] ^(g)	5	220	4-40	?
B [μG] ^(h)	10-1000	1-100	?	?
Metallicity, Z ⁽ⁱ⁾	2	1	~ 2	0.2-0.6
CRIR [$\log_{10}(s^{-1})$] ^(j)	-15 to -13	-17 to -15	?	?
Linewidth, $\sigma(10\text{pc})$ [km s^{-1}] ^(l)	12	3	10	20-70
Linewidth scaling, b ^(m)	0.7	0.5	?	?
IMF slope, α ⁽ⁿ⁾	≤ 2.35	2.35	?	?
DGMF, $f(n > 10^4)$ ^(o)	0.95	0.03	?	?
T_{gas} [K] ^(p)	50-100	10-30	50-250	?
T_{dust} [K] ^(q)	20-50	10-30	30-45	?
$P_{\text{ext}}/k_{\text{B}}$ [K cm^{-3}] ^(r)	$\gtrsim 10^7$	$\gtrsim 10^5$	10^6-10^8	?

Open questions in Galactic Center star formation

- How do stars form in the Galactic Center?
- Why is star formation in the GC different than in the Galactic disk?
- What are the initial conditions for SF in the GC?
- What role do chemistry, turbulence, and gas kinematics play in GC SF?
- Why is The Brick forming so few stars?

Henshaw+2023



Tafalla+2021

MUSTANG Galactic Plane Survey (MGPS90)

- 90 GHz, 9" resolution
- Data processing by Charles Romero and Simon Dicker
- 709 sources over 7 fields from $0^\circ < l < 50^\circ$
- Recovered several HCHII regions, some new candidates
- Relevant part for me: G01 field (see right), covered Sgr B2 and The Brick

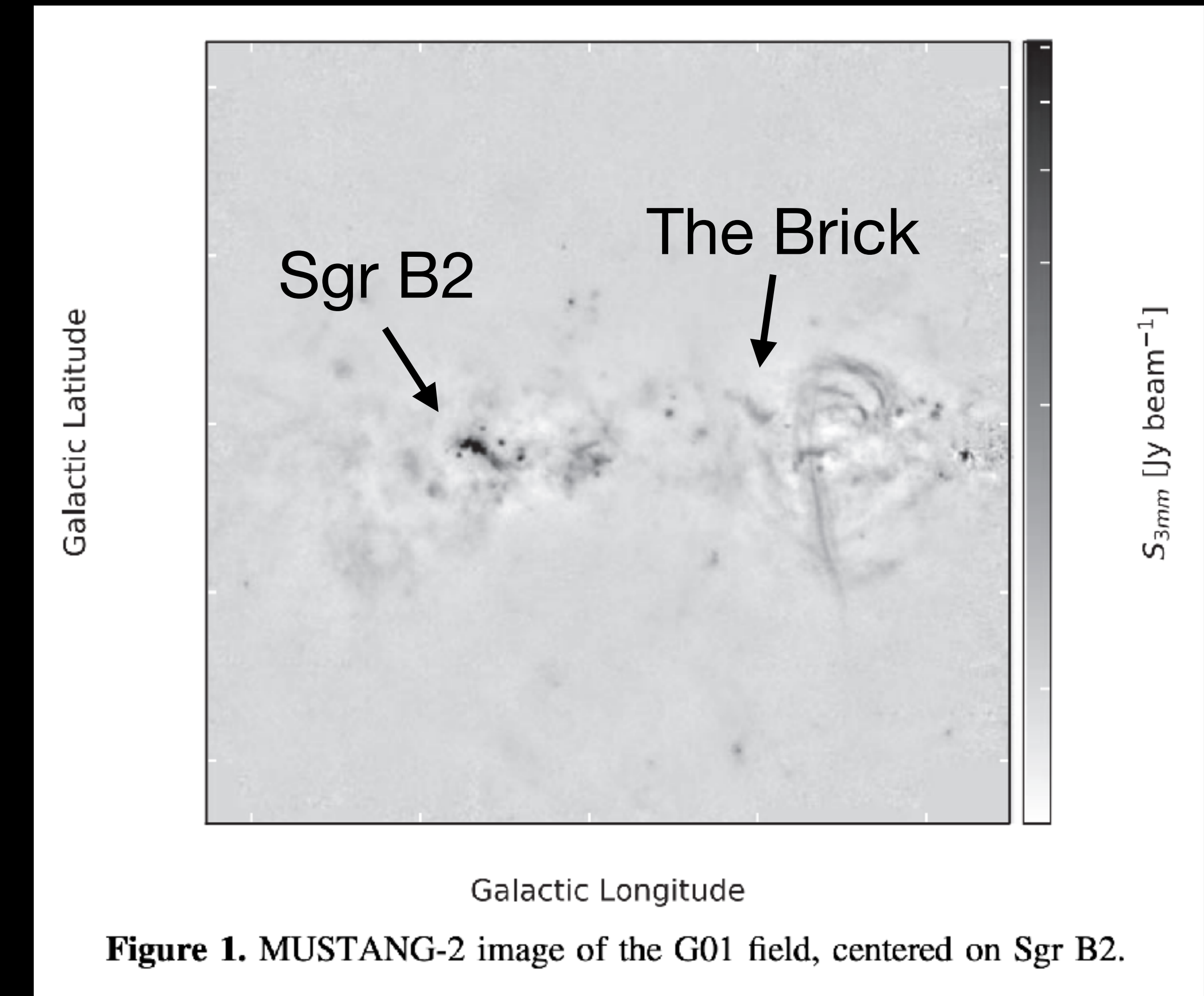


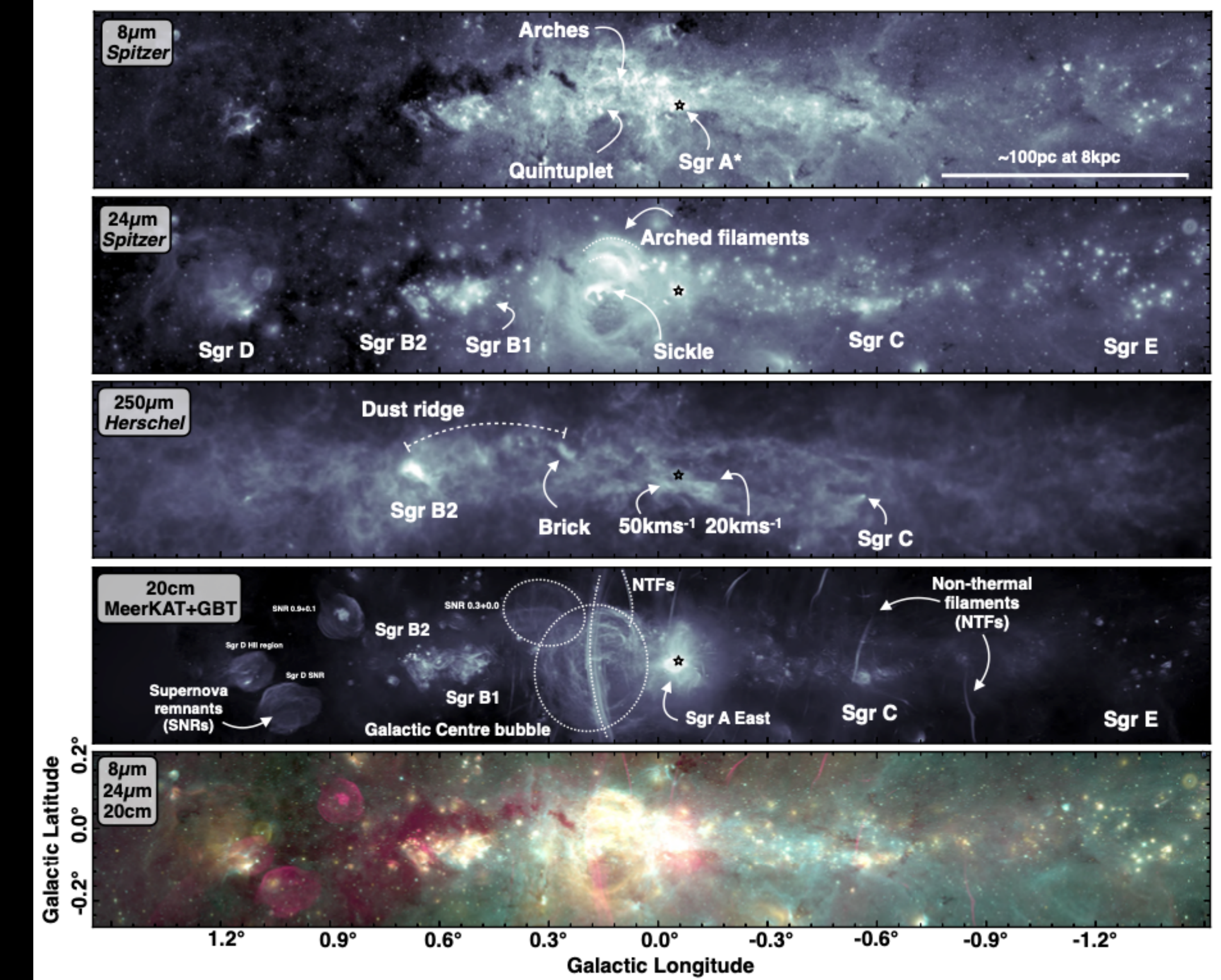
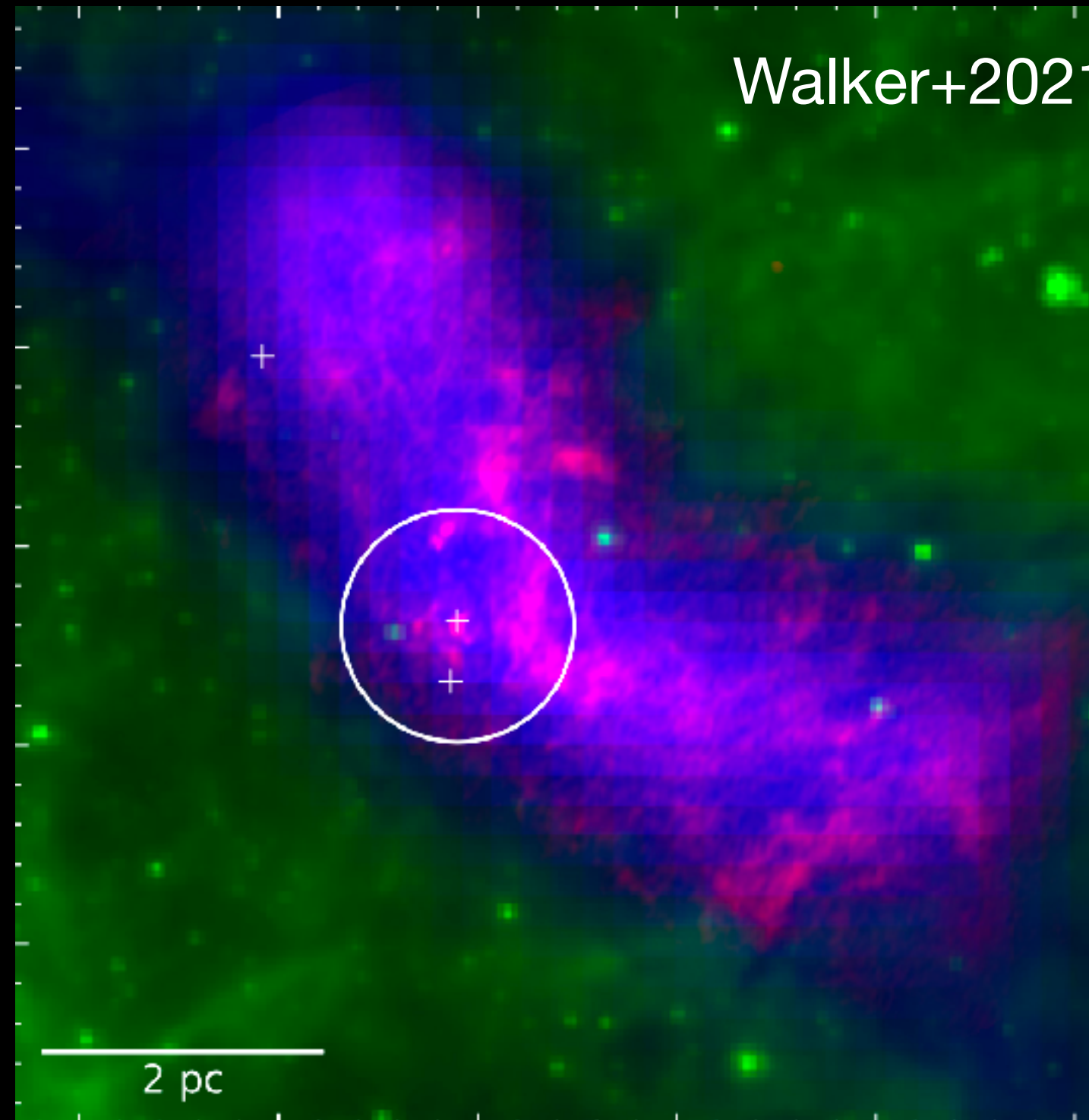
Figure 1. MUSTANG-2 image of the G01 field, centered on Sgr B2.

Ginsburg+2020

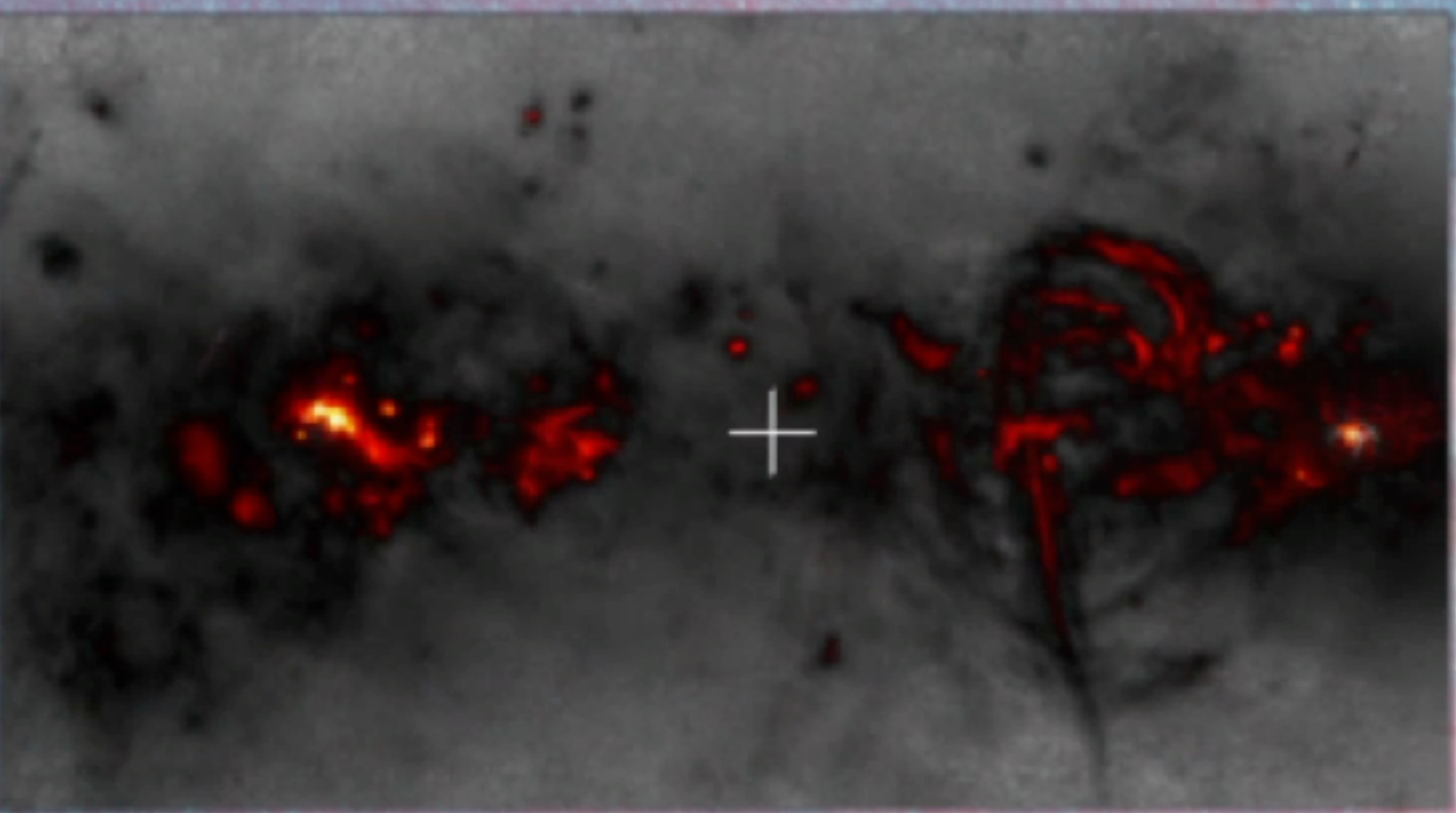


G0.253+0.016

The Brick



Zoom-in on The Brick

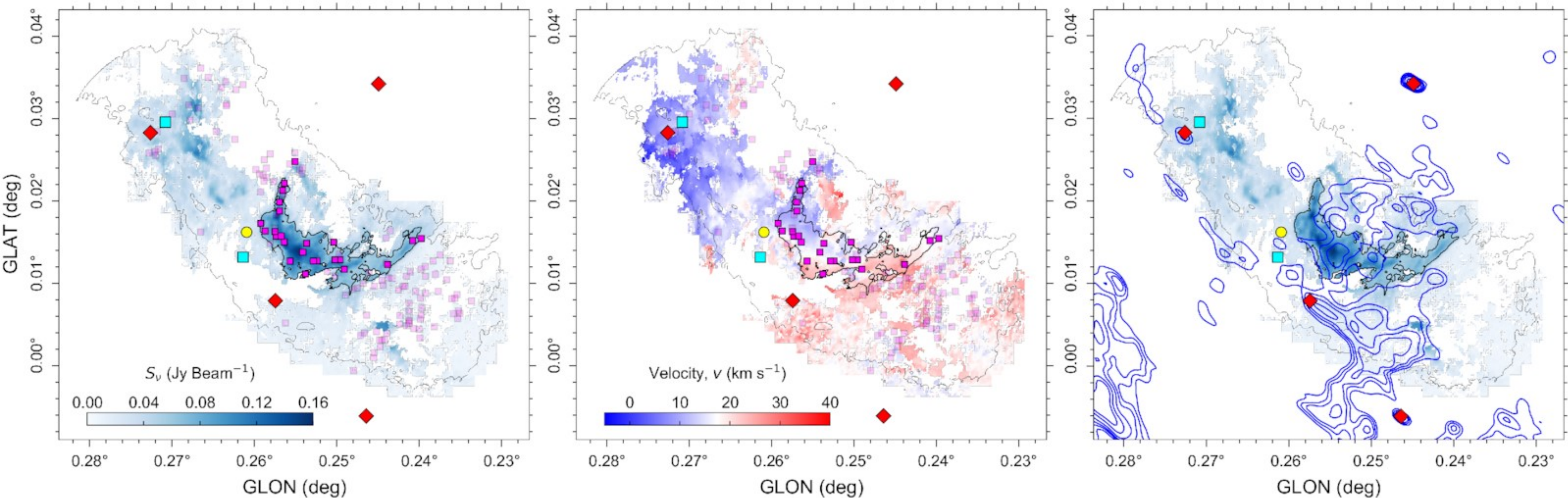


Recent science on The Brick

- A wind-blown bubble in the Central Molecular Zone cloud G0.253+0.016 (Henshaw+2022, incl. Bulatek)



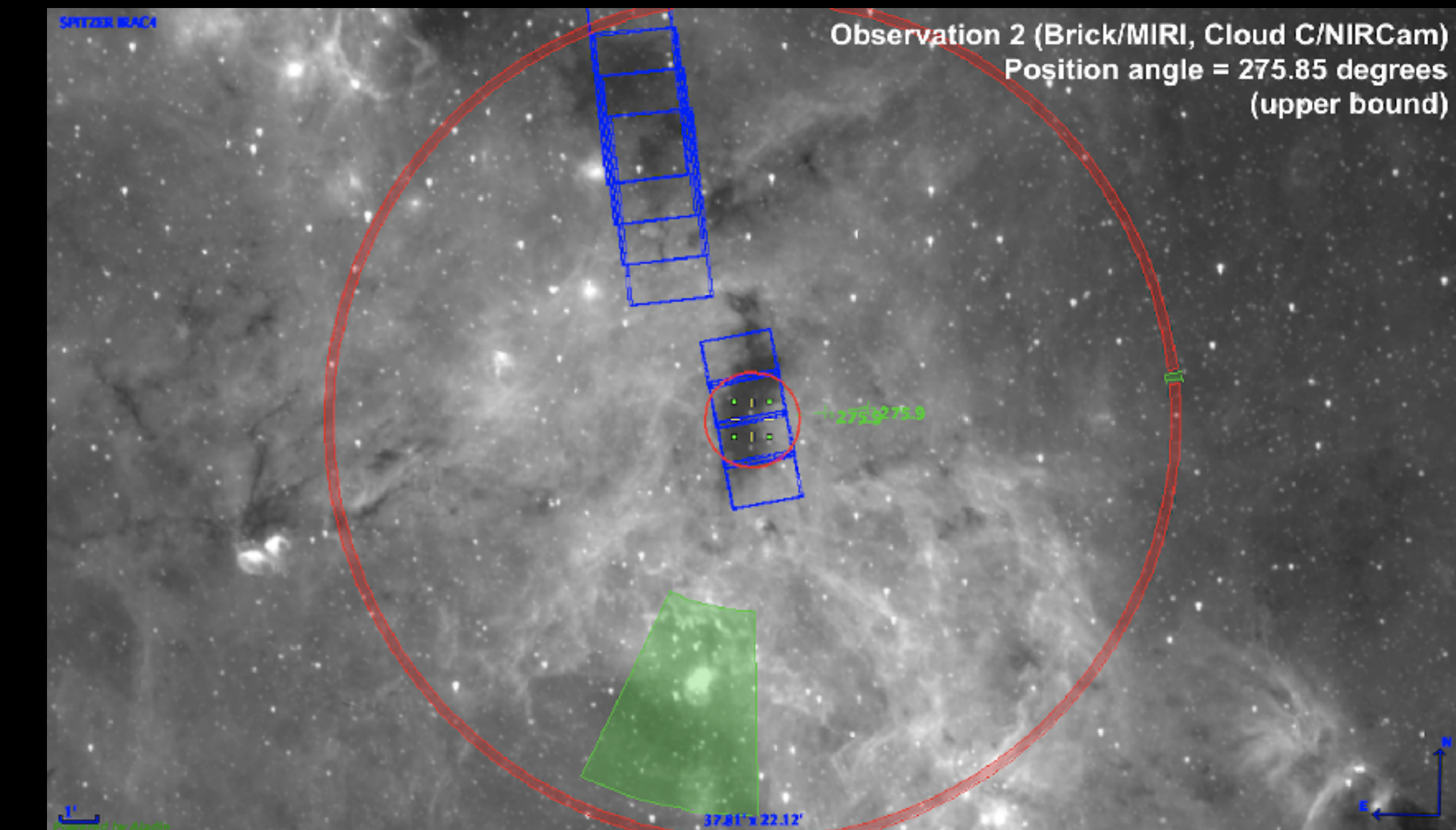
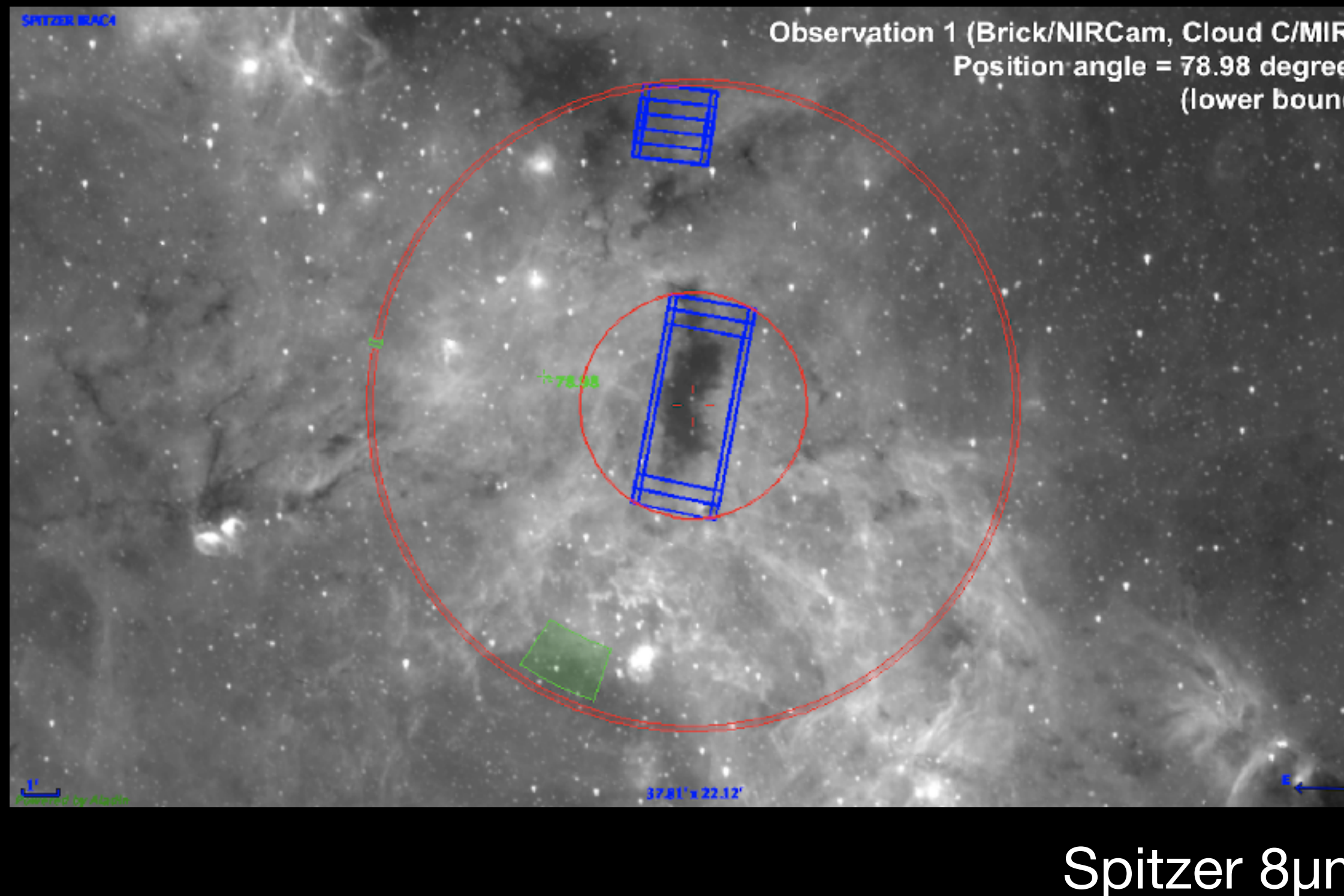
and Mopra



Recent science on The Brick



- JWST Reveals Widespread CO Ice and Gas Absorption in the Galactic Center Cloud G0.253+0.016 (Ginsburg+2023, incl. Bulatek)



Recent science on The Brick



- JWST Reveals Widespread CO Ice and Gas Absorption in the Galactic Center Cloud G0.253+0.016 (Ginsburg+2023, incl. Bulatek)

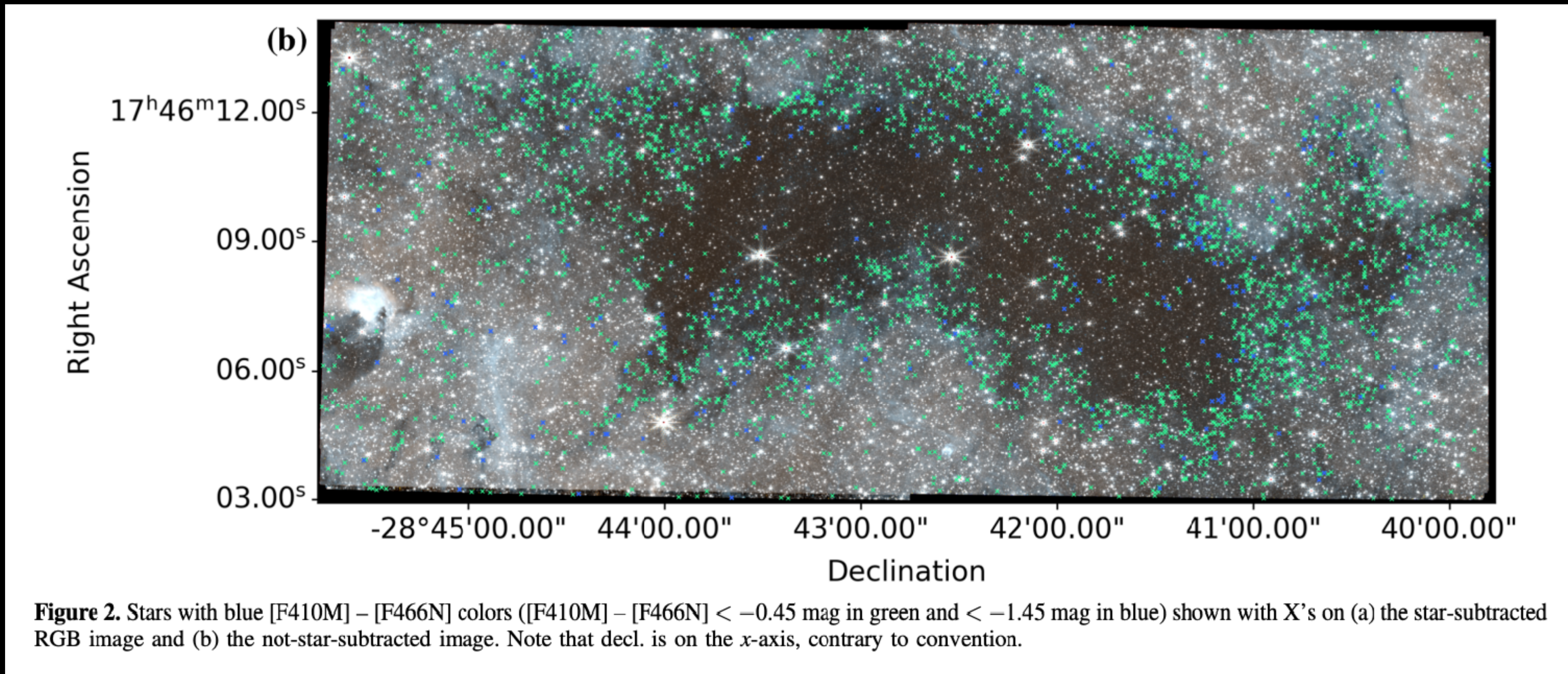
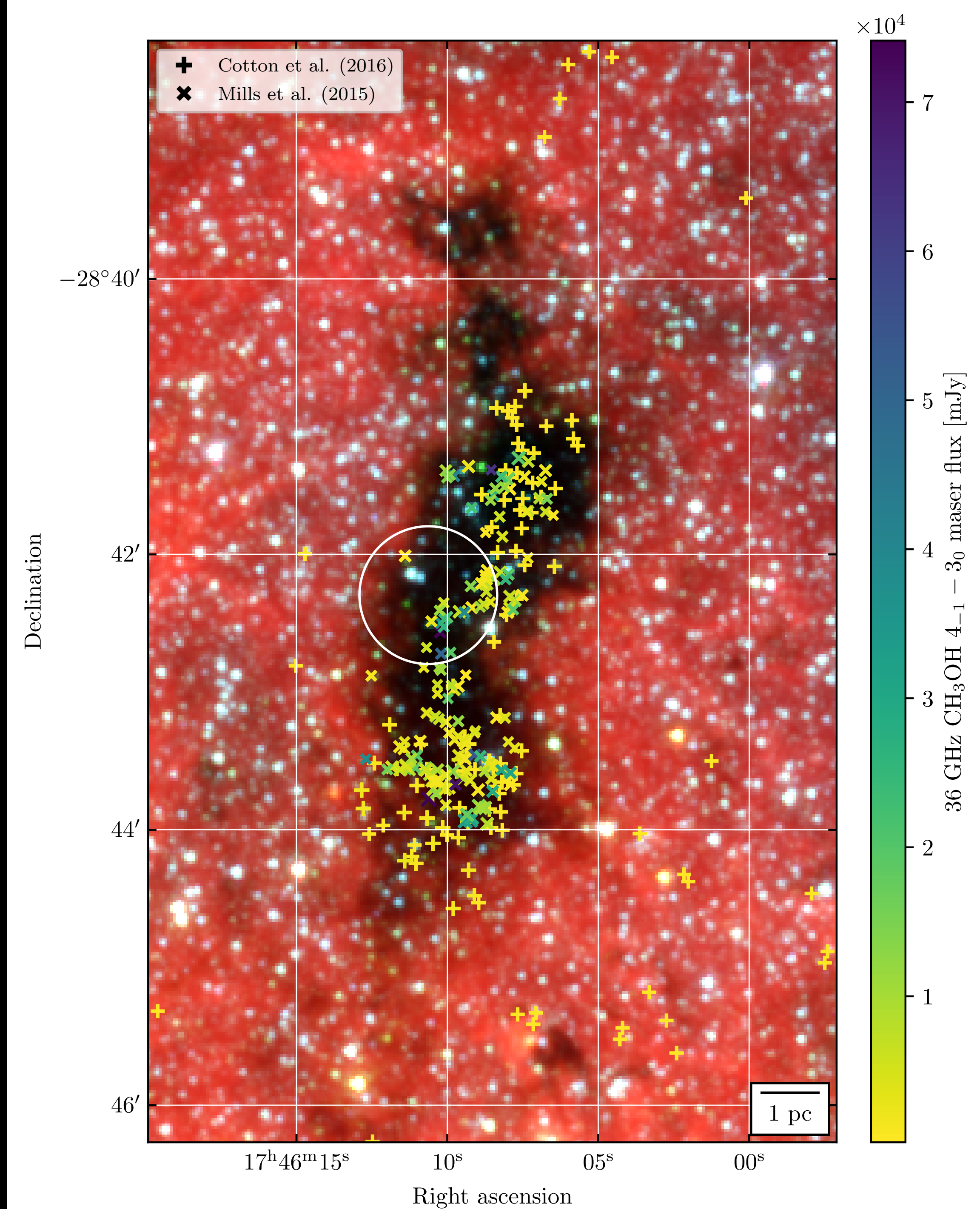


Figure 2. Stars with blue [F410M] – [F466N] colors ($[F410M] - [F466N] < -0.45$ mag in green and < -1.45 mag in blue) shown with X's on (a) the star-subtracted RGB image and (b) the not-star-subtracted image. Note that decl. is on the x-axis, contrary to convention.

The Brick Line Survey

Bulatек+ in prep.

- Which spectral lines trace what physical processes in the Galactic Center?
- ALMA Bands 3, 4, 6
- 1'' angular res.,
~0.25 K sensitivity
in 1 km/s channel
- LAS = 5'' – 10''

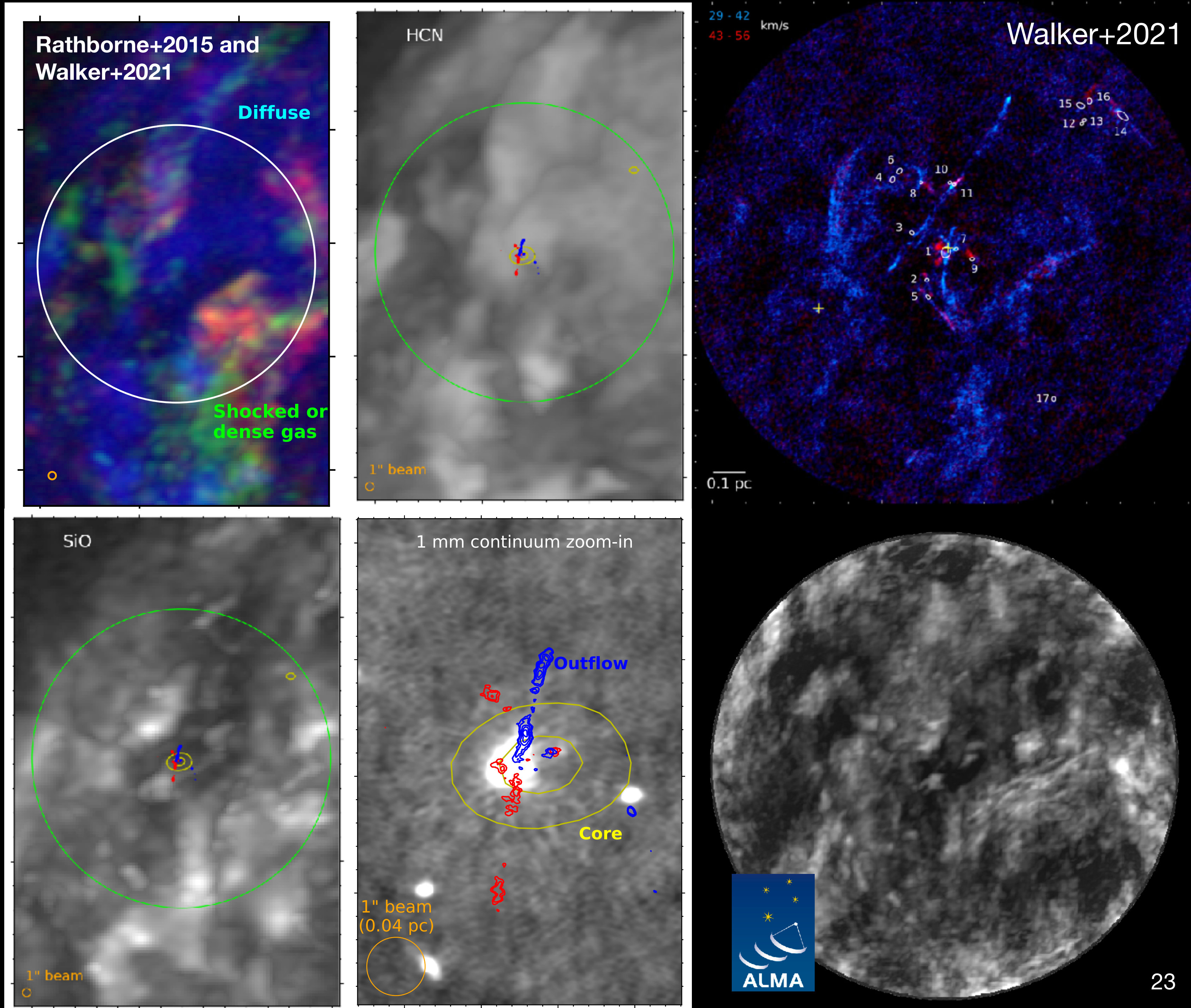


BL5

The Brick Line Survey

Bulatек+ in prep.

- Which spectral lines trace what physical processes in the Galactic Center?
- ALMA Bands 3, 4, 6
- 1'' angular res., ~0.25 K sensitivity in 1 km/s channel
- LAS = 5'' – 10''



Molecular excitation
(we found a dasar)

CH₃OH

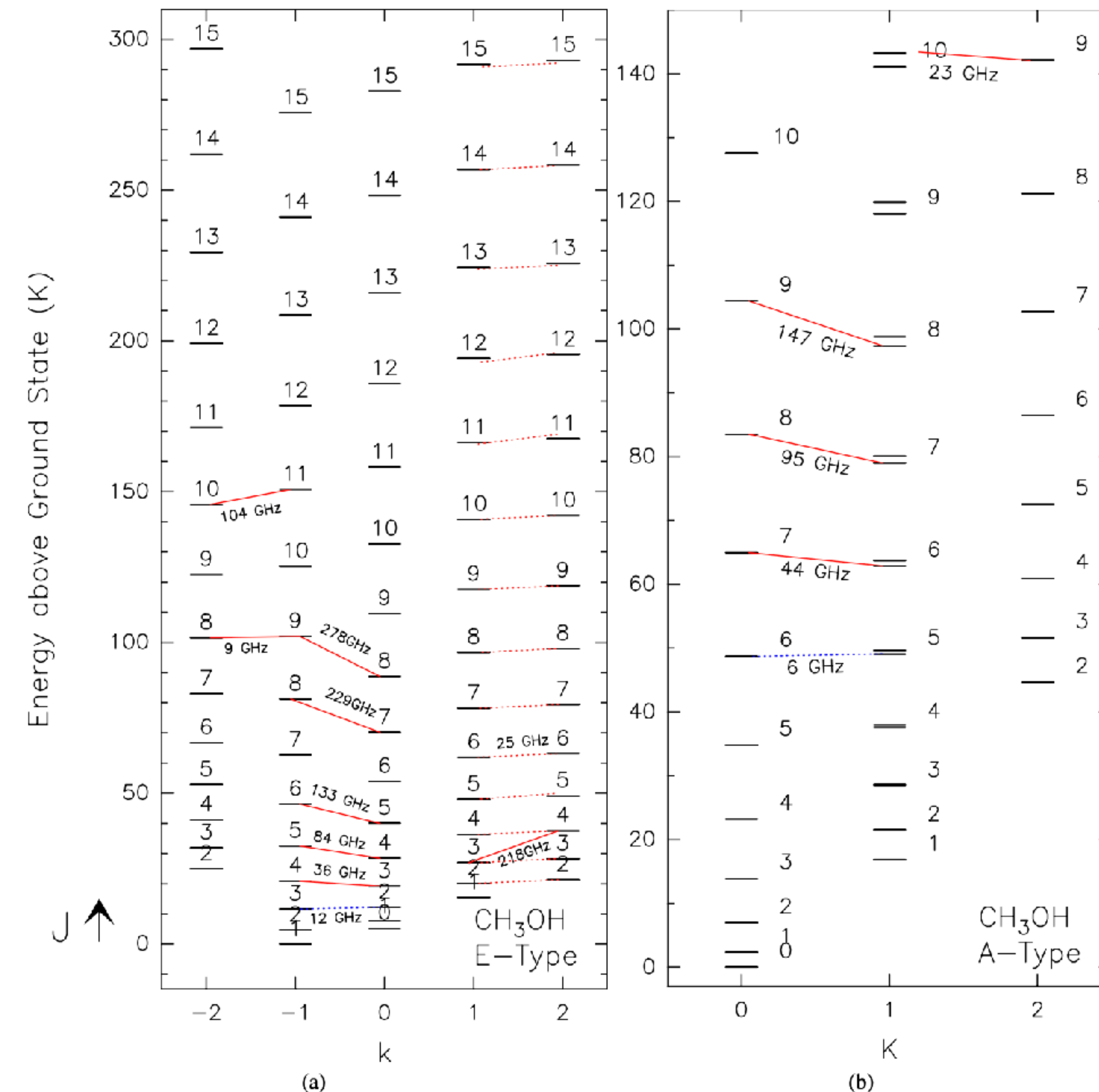
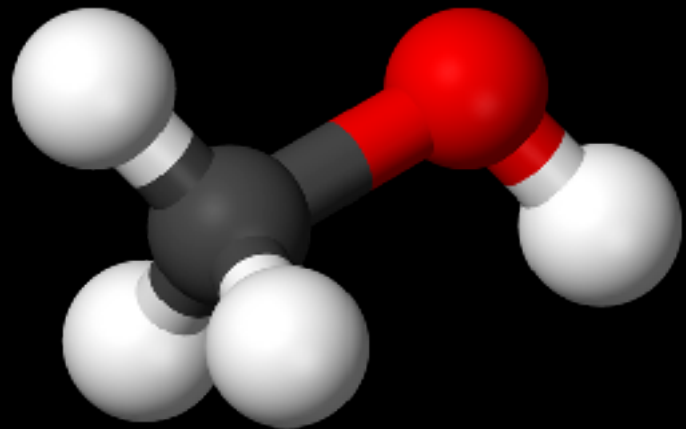
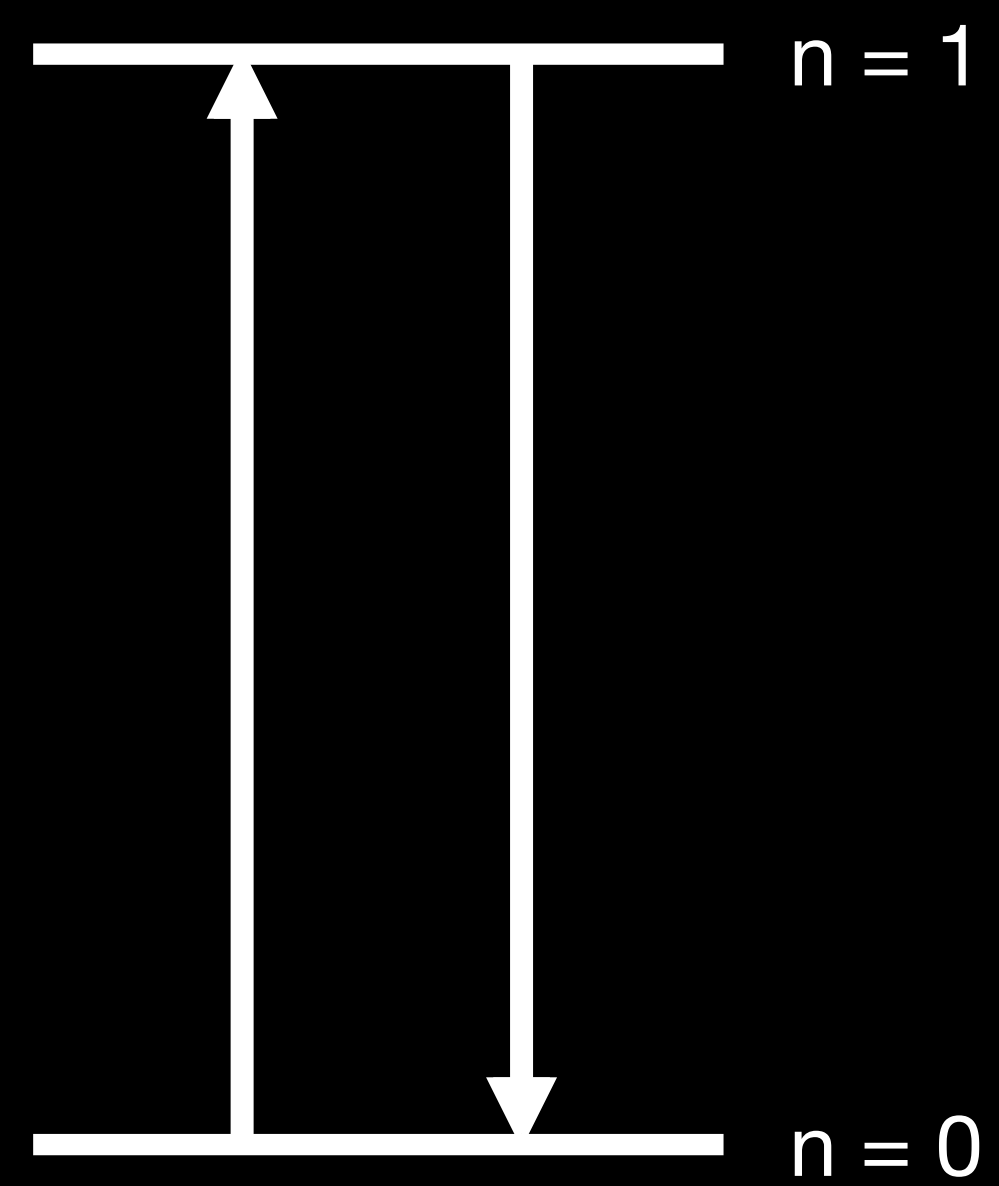


Fig. 3. Partial rotational level diagram of *E*-type (left) and *A*-type methanol (right). Known Class I maser transitions are connected by red lines with frequencies indicated; blue dotted lines connect anti-inverted transitions. We note that all of the maser lines originating in the $J_2 \rightarrow J_1 E$ series near 25 GHz are indicated by dotted red lines.

Methanol Dasar in The Brick

Bulatek et al. 2023, ApJ, 956, 2

- MASER = Microwave Amplification by Stimulated Emission of Radiation
 - Population inversion: excess population of molecules in upper energy state
 - A photon knocks a molecule out of the upper state
 - Needs source of coherent amplification
- DASAR = Dark "Amplification" by "Stimulated" Absorption of Radiation
 - Pump drives molecules into lower energy state, that then absorb photons

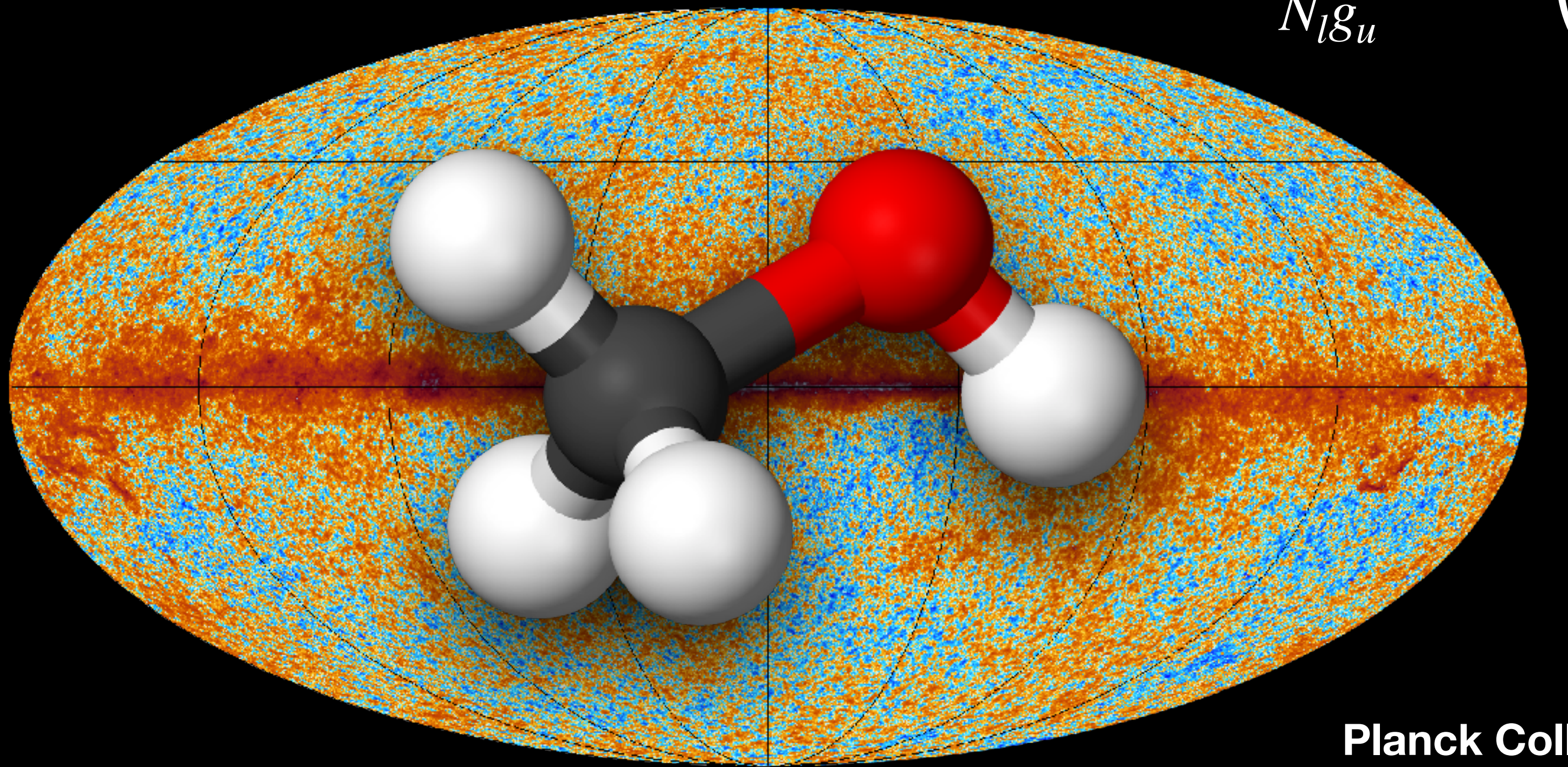


$$\frac{N_u g_l}{N_l g_u} = \exp\left(\frac{-\Delta E}{k_B T_{ex}}\right)$$

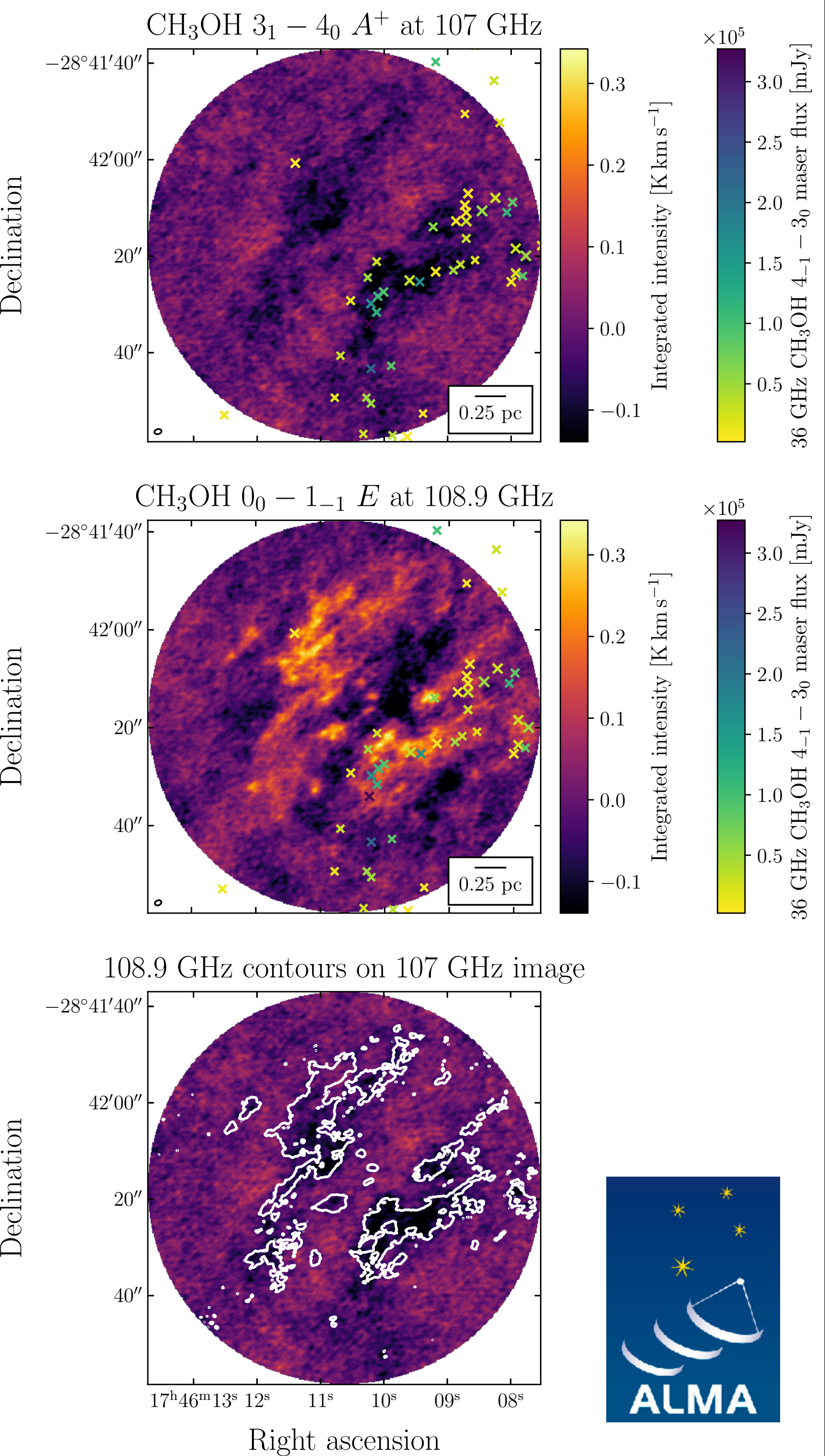
Methanol Dasar in The Brick

Bulatek et al. 2023, ApJ, 956, 2

- If the pump gets T_{ex} cold enough, the molecule could even absorb the CMB!



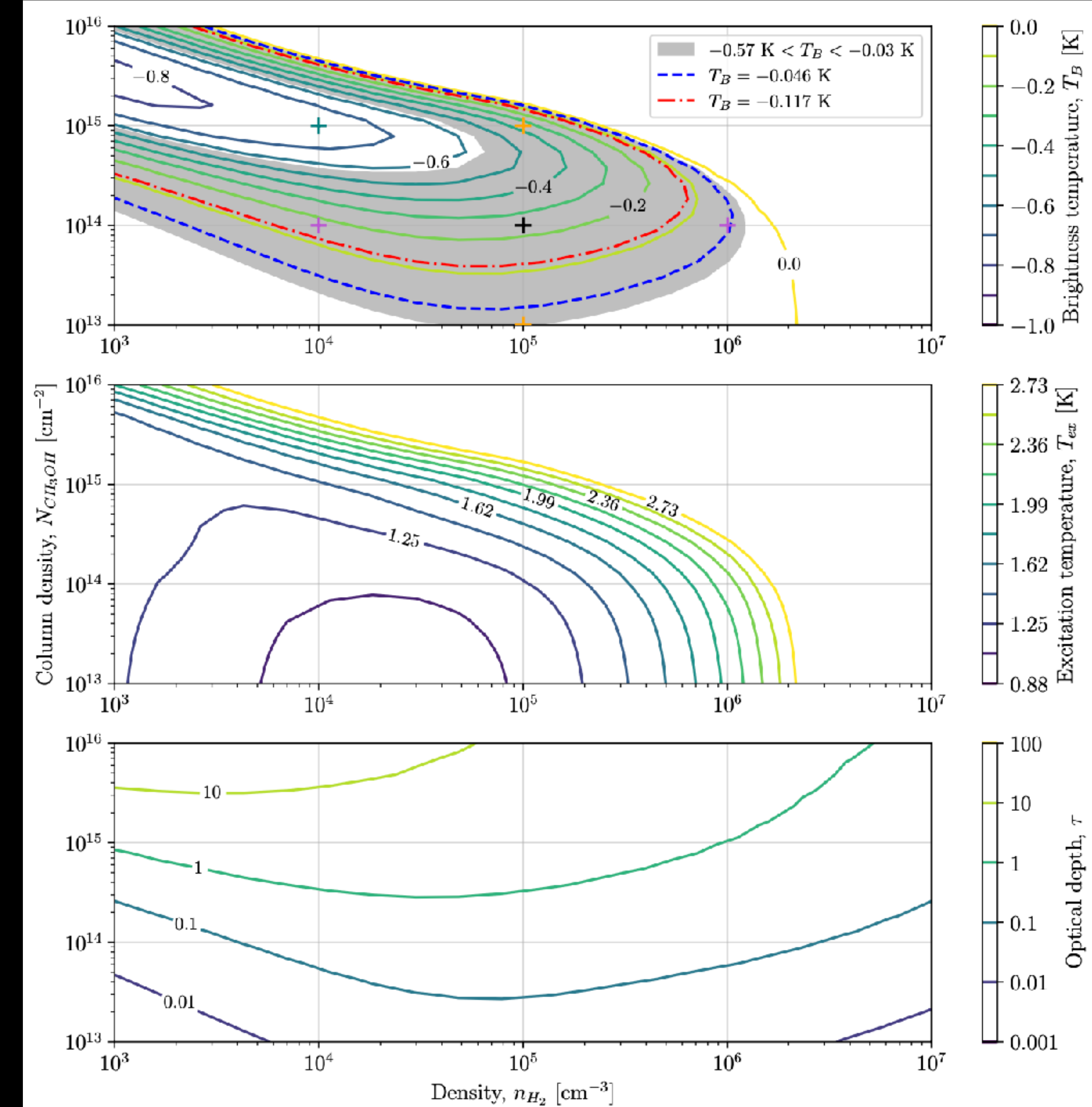
$$\frac{N_u g_l}{N_l g_u} = \exp\left(\frac{-\Delta E}{k_B T_{ex}}\right)$$



Methanol Dasar in The Brick

Bulatek+2023

- Modeled dasing volume density, column density, and temperature using RADEX
- Evaluated the use of this line for detecting/measuring dasing regions in high-redshift galaxies
 - Preference for edge-on spirals
 - The ngVLA will be able to observe this line (and others) in starburst galaxies up to at least $z = 5$



GBT is a powerhouse for formaldehyde dasars

- Formaldehyde Densitometry of Starburst Galaxies (Mangum+2008)

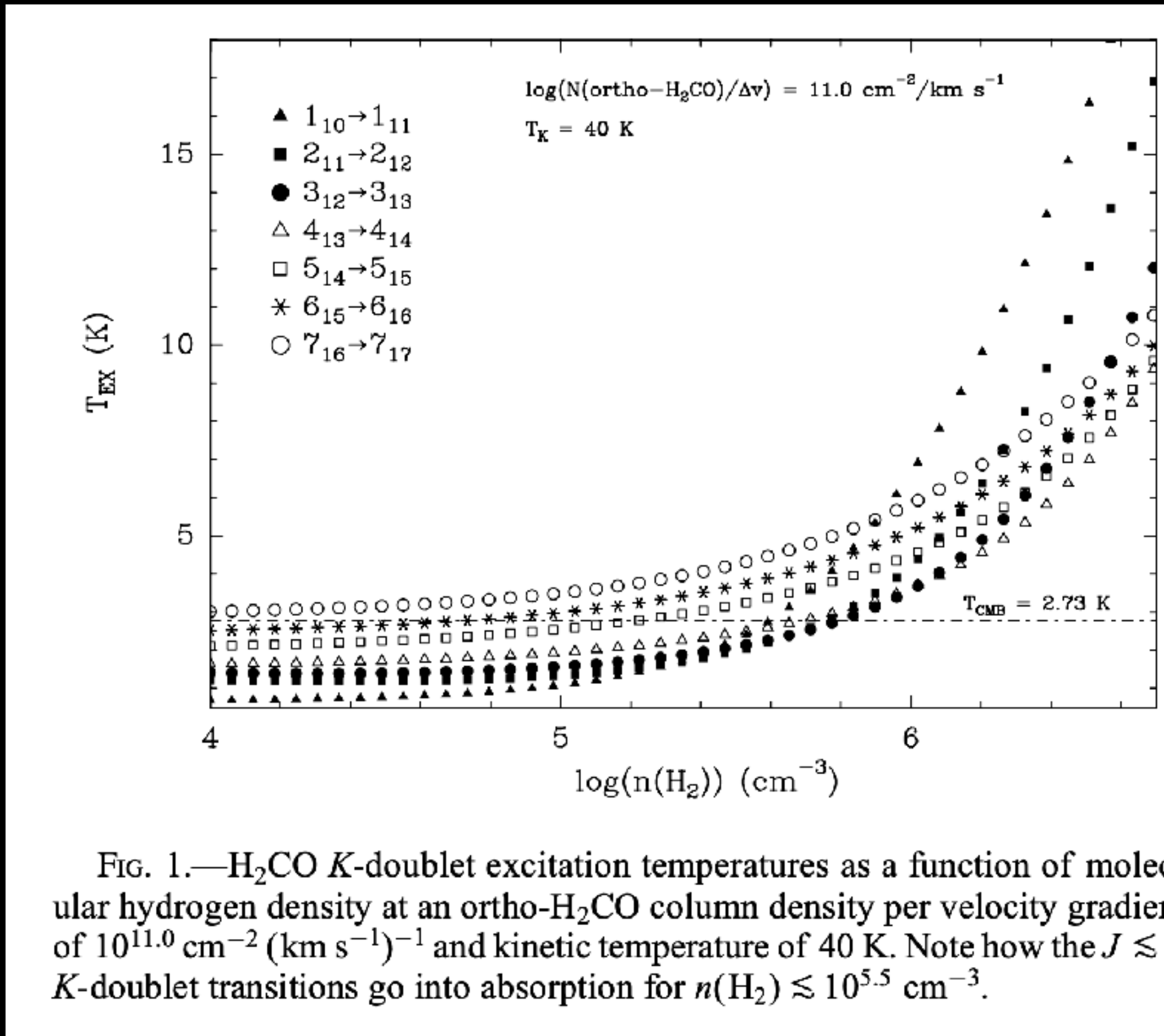


FIG. 1.— H_2CO K -doublet excitation temperatures as a function of molecular hydrogen density at an ortho- H_2CO column density per velocity gradient of $10^{11.0} \text{ cm}^{-2} (\text{km s}^{-1})^{-1}$ and kinetic temperature of 40 K. Note how the $J \lesssim 5$ K -doublet transitions go into absorption for $n(\text{H}_2) \lesssim 10^{5.5} \text{ cm}^{-3}$.

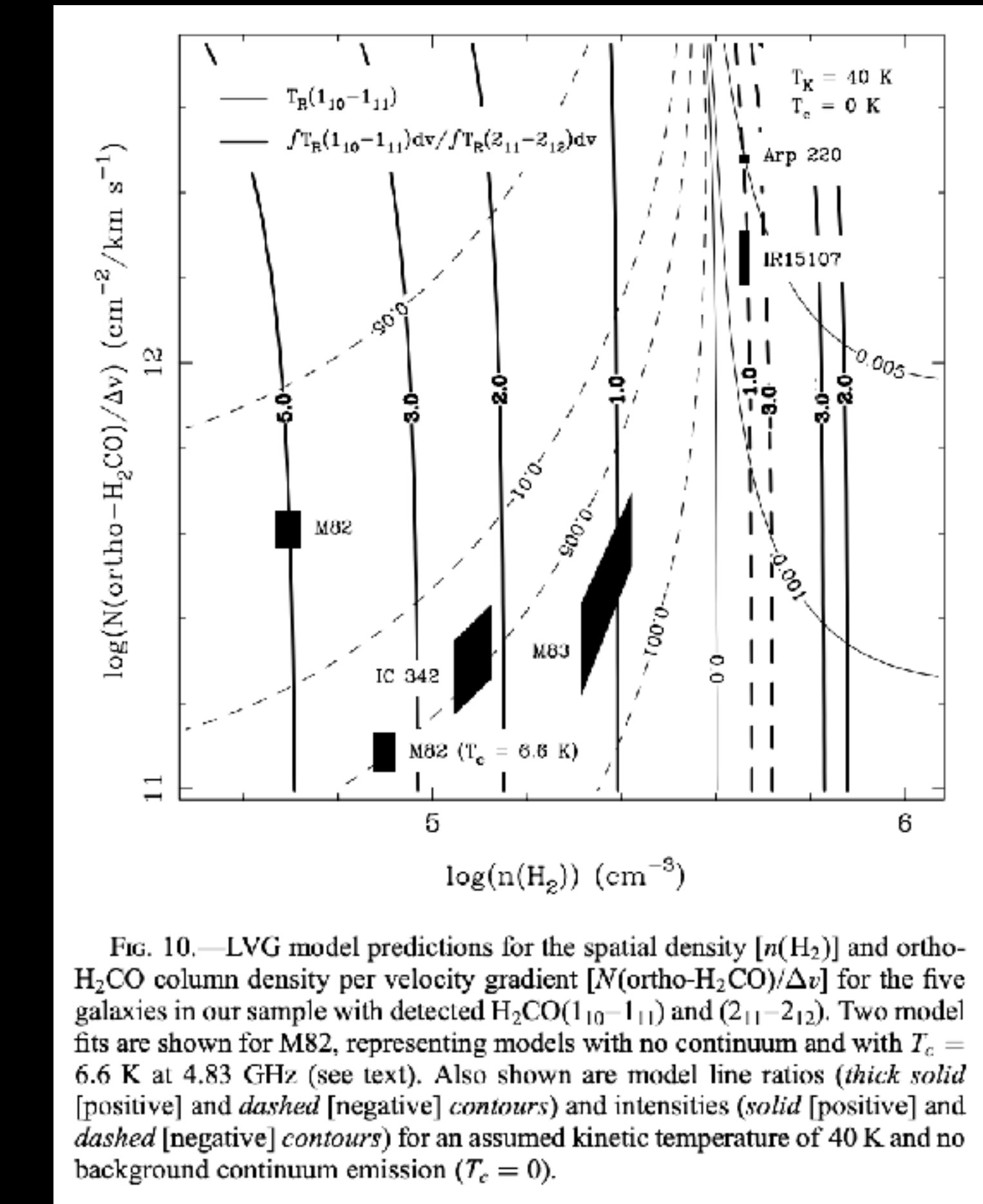


FIG. 10.—LVG model predictions for the spatial density [$n(\text{H}_2)$] and ortho- H_2CO column density per velocity gradient [$N(\text{ortho-H}_2\text{CO})/\Delta v$] for the five galaxies in our sample with detected $\text{H}_2\text{CO}(1_{10}-1_{11})$ and $(2_{11}-2_{12})$. Two model fits are shown for M82, representing models with no continuum and with $T_c = 6.6 \text{ K}$ at 4.83 GHz (see text). Also shown are model line ratios (thick solid [positive] and dashed [negative] contours) and intensities (solid [positive] and dashed [negative] contours) for an assumed kinetic temperature of 40 K and no background continuum emission ($T_c = 0$).

GBT is a powerhouse for formaldehyde dasars

- Formaldehyde Anti-Inversion at $z = 0.68$ in the Gravitational Lens B0218+357 (Zeiger & Darling 2010)

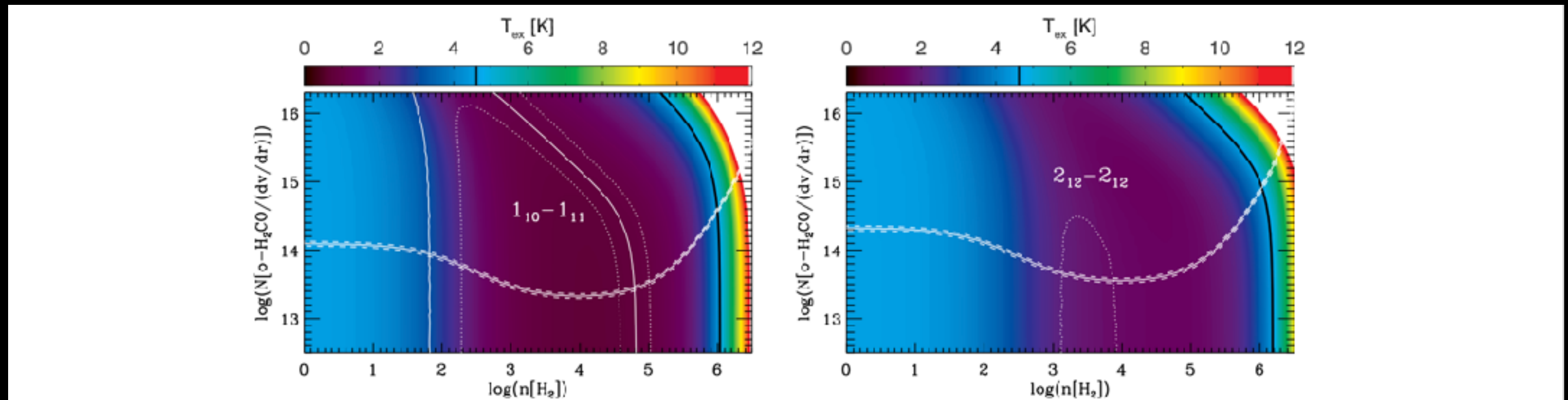


Figure 3. Contours trace excitation temperatures of the $1_{10}-1_{11}$ (left) and $2_{11}-2_{12}$ (right) transitions as a function of $n(\text{H}_2)$ and $N(\text{o-H}_2\text{CO})/(\text{km s}^{-1} \text{ pc}^{-3})^{-1}$ as calculated with our LVG model. Overplotted white lines represent the observed peak optical depth of the $1_{10}-1_{11}$ line (\sim horizontal) and the ratio of observed peak optical depths of the $1_{10}-1_{11}$ and $2_{11}-2_{12}$ lines (\sim vertical) with 68% (1σ) confidence intervals. $T_{\text{CMB}} = 4.6 \text{ K}$ at $z = 0.68$, which we set as the background radiation temperature, and $T_{\text{kin}} = 55 \text{ K}$ (Henkel et al. 2005). The black line is the 4.6 K contour. CS observations and modeling firmly limit $n(\text{H}_2) < 2 \times 10^4 \text{ cm}^{-3}$ (Henkel et al. 2005)—the range of these plots exceed that limit to show the behavior of H_2CO as a function of $n(\text{H}_2)$ —and $T_{\text{ex}} < T_{\text{CMB}}$ for all points on the map below that limit. Column density (y-axis) is in units of $\text{cm}^{-2} (\text{km s}^{-1} \text{ pc}^{-3})^{-1}$, and number density (x-axis) is in units of cm^{-3} . It is assumed throughout this paper that the velocity gradient dv/dr is $1 \text{ km s}^{-1} \text{ pc}^{-1}$. The white at high $n(\text{H}_2)$ represents a ceiling to the contours at 12 K and not a physical plateau. The upper right corner of the $1_{10}-1_{11}$ plot reaches $\sim 55 \text{ K}$, the kinetic temperature of the gas. Overplotted white lines on the $1_{10}-1_{11}$ plot represent the solution if covering factors are $f_{4.8} = 0.5$ and $f_{14.5} = 0.8$; the central region is excluded, while a cloud with negligible collisions— $\log(n[\text{H}_2]) = 0 \text{ cm}^{-3}$ —but unrealistic X is not excluded by the ratio of optical depths at the 68% confidence level if priors on X are neglected. The similar lines on the $2_{11}-2_{12}$ plot represent the constraints placed by observations if covering factors are $f_{4.8} = 0.3$ and $f_{14.5} = 1.0$; the central region is within the 68% confidence region although there is no solution in the model that exactly matches the observed lines. Differences in solutions shown on the two plots are due entirely to the selection of covering factors.

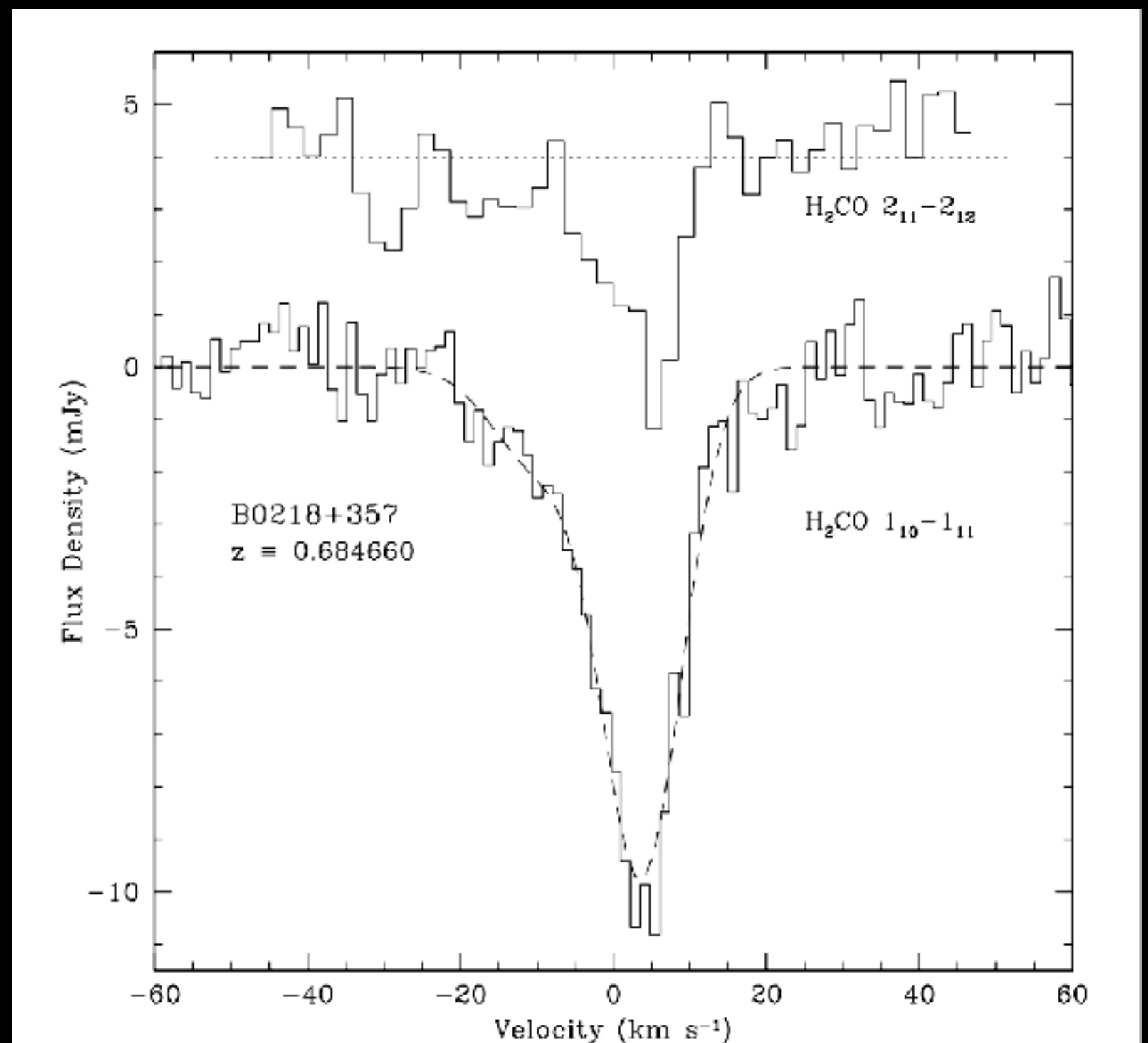
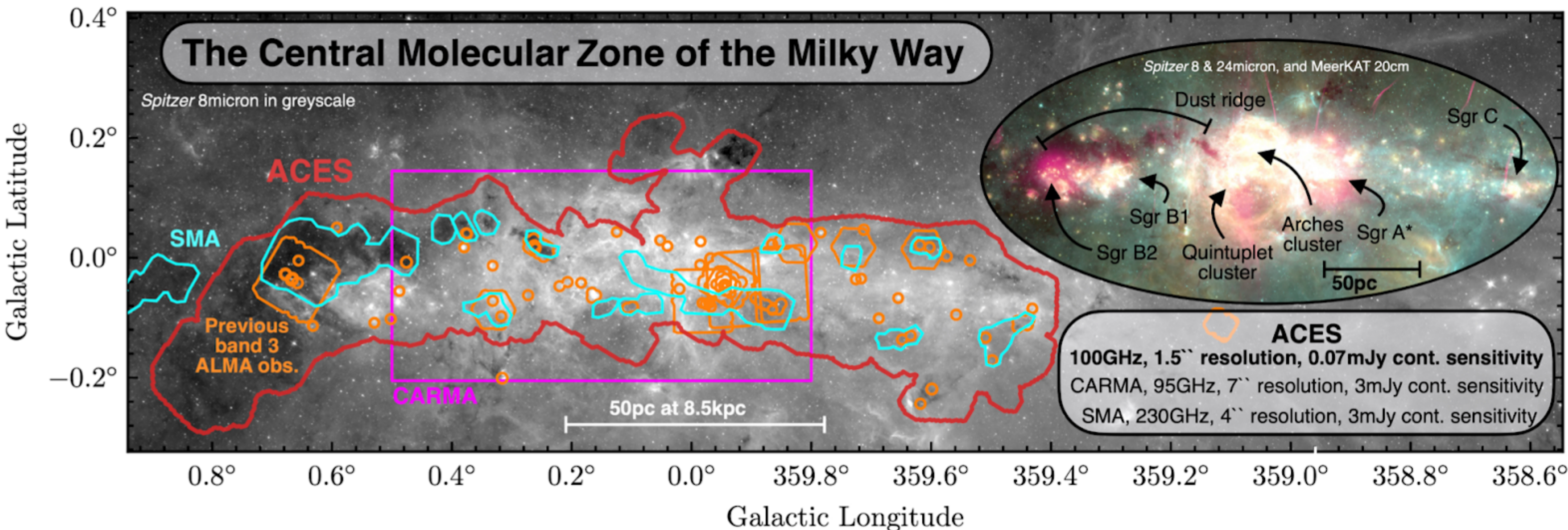


Figure 2. Formaldehyde $1_{10}-1_{11}$ (6 cm) and $2_{11}-2_{12}$ (2 cm) absorption toward the gravitational lens system B0218 + 357. The rest-frame velocity scale assumes a heliocentric redshift of $z = 0.684660$, and the spectral resolutions are 1.3 and 2.1 km s^{-1} in the lower and upper lines, respectively. The dashed line shows a two-component Gaussian fit to the 6 cm line profile. The 2 cm line spectrum, also detected by Menten & Reid (1996), is offset by 4 mJy , with the zero point indicated by the dotted line.

Why am I at Green Bank?

The ALMA CMZ Exploration Survey

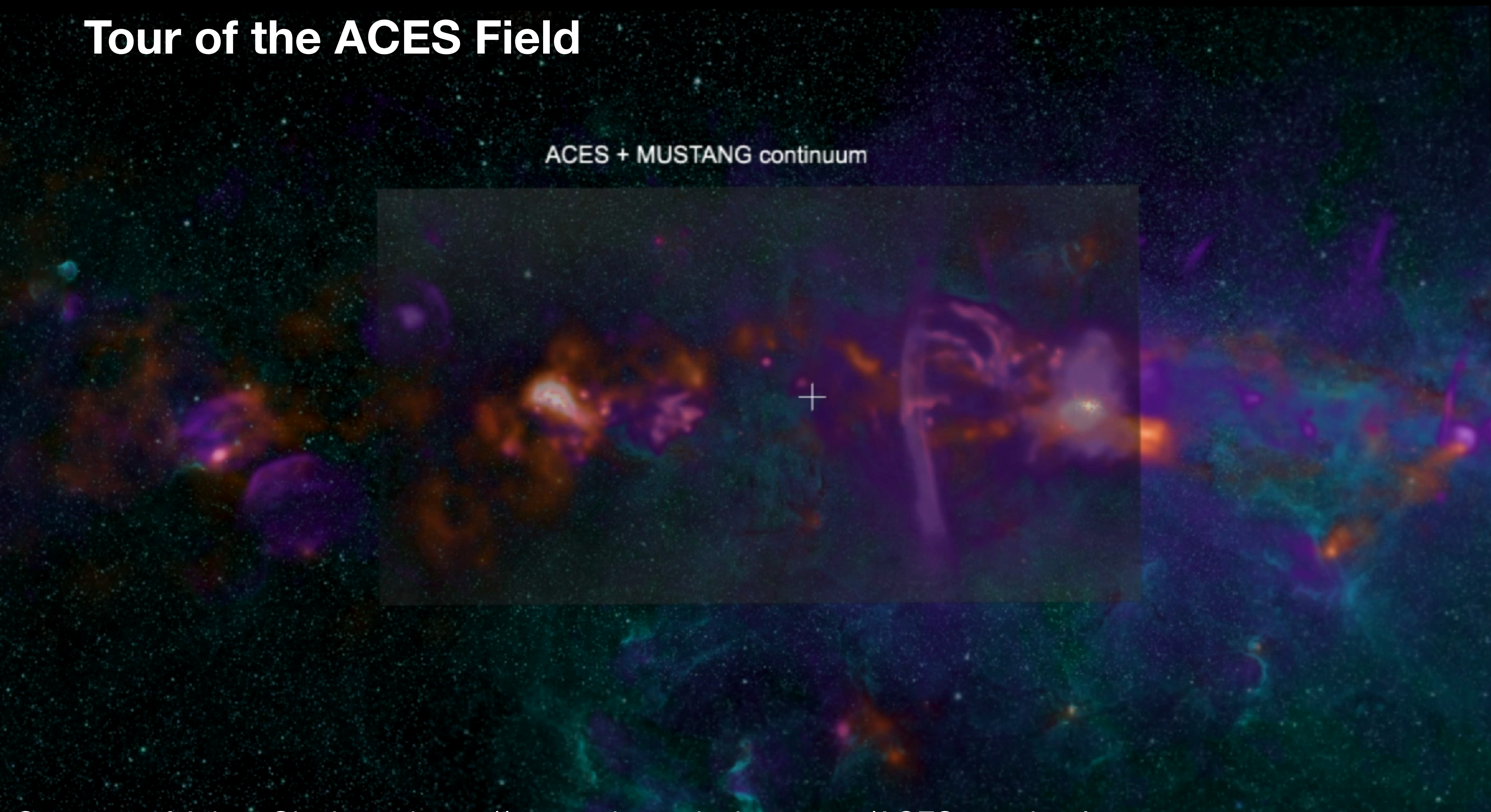
ACES, 2021.1.00172.L (PI: Longmore)



Composite image made by ACES Collaboration

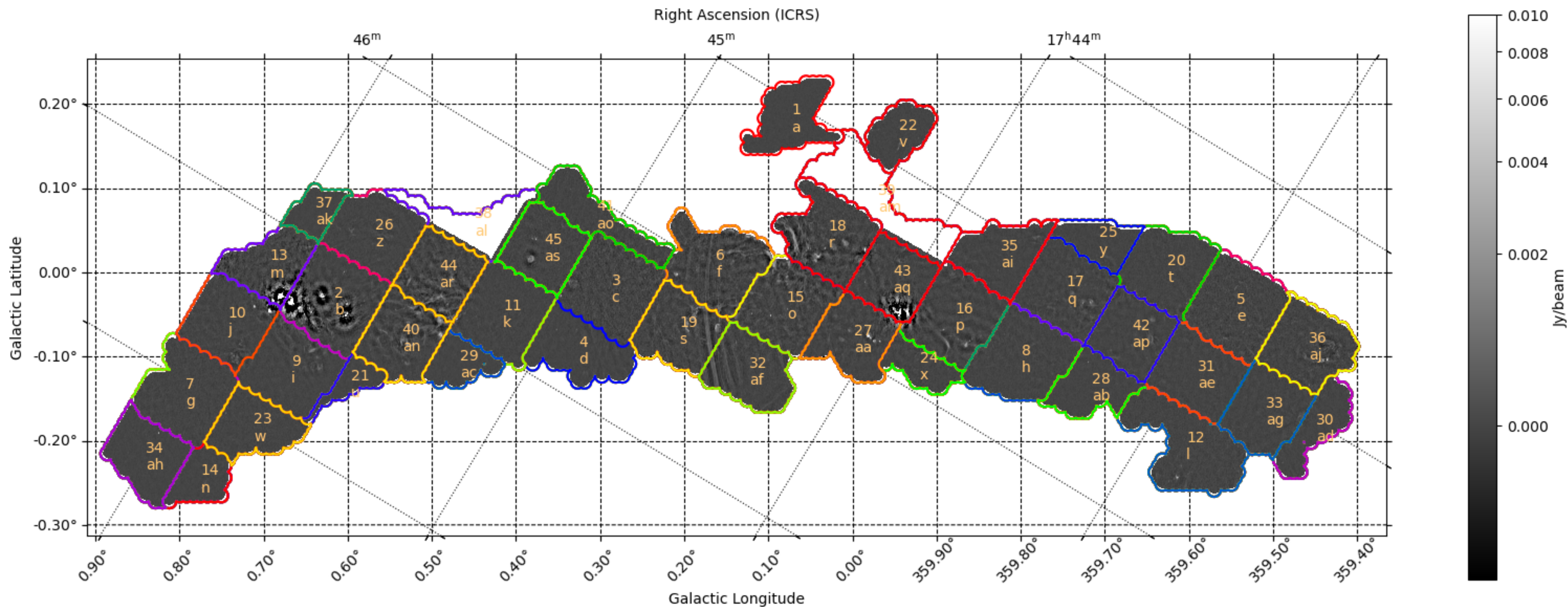
Tour of the ACES Field

ACES + MUSTANG continuum



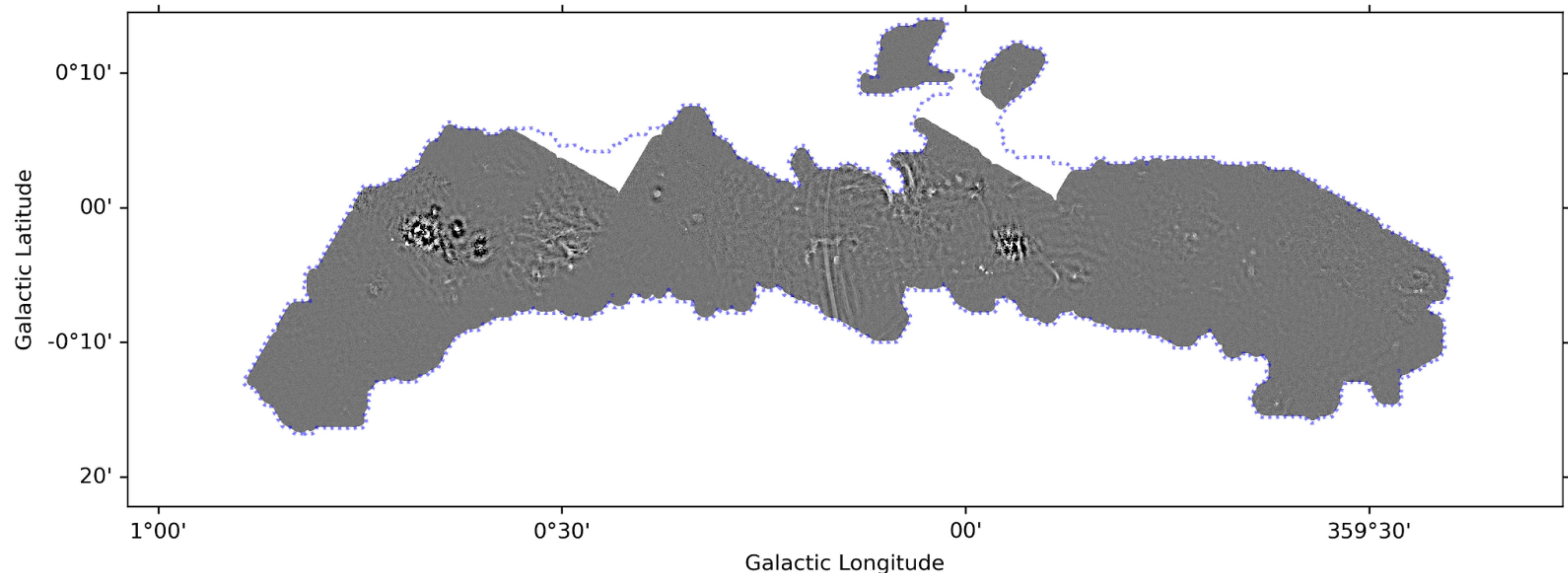
Observing breakdown

ACES

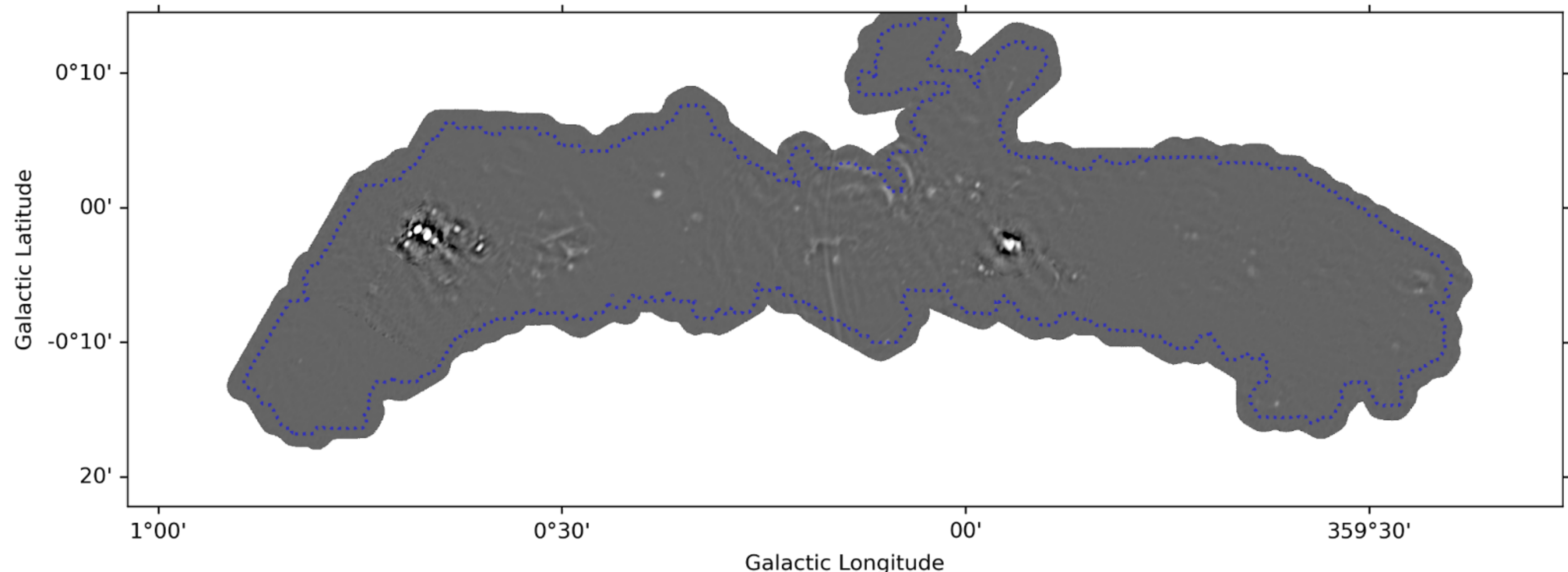


12-m continuum

ACES

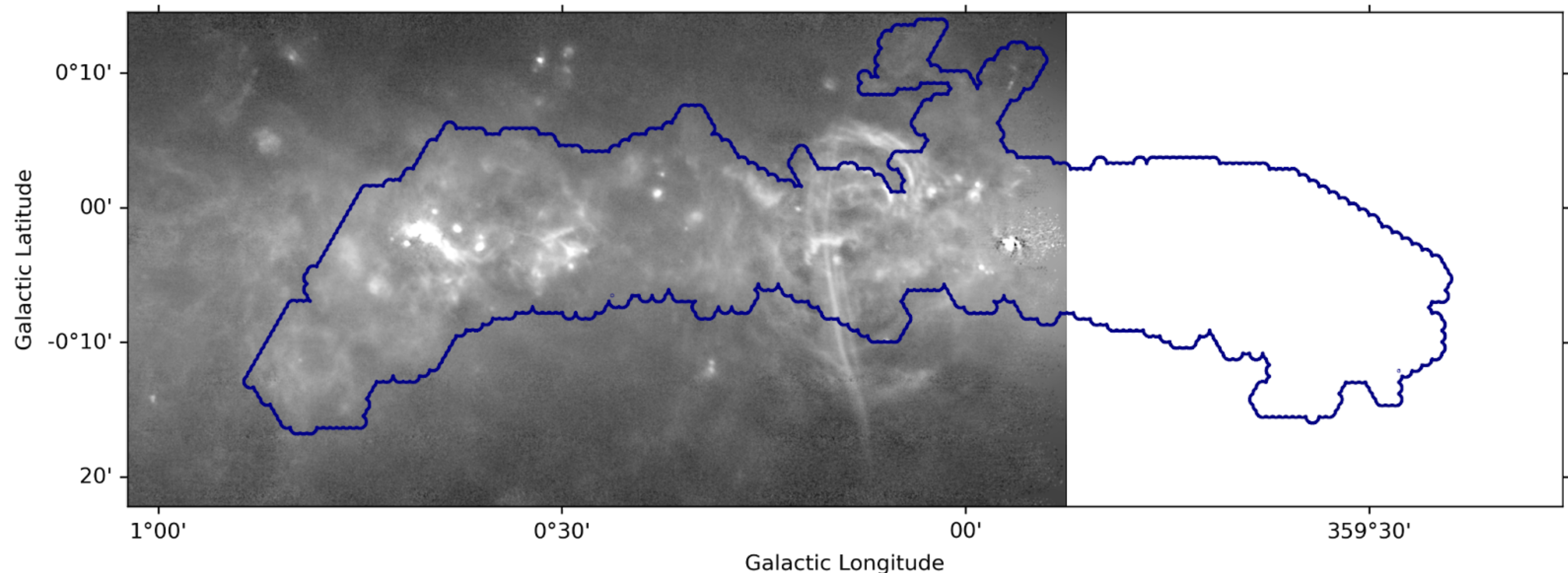


7-m continuum ACES

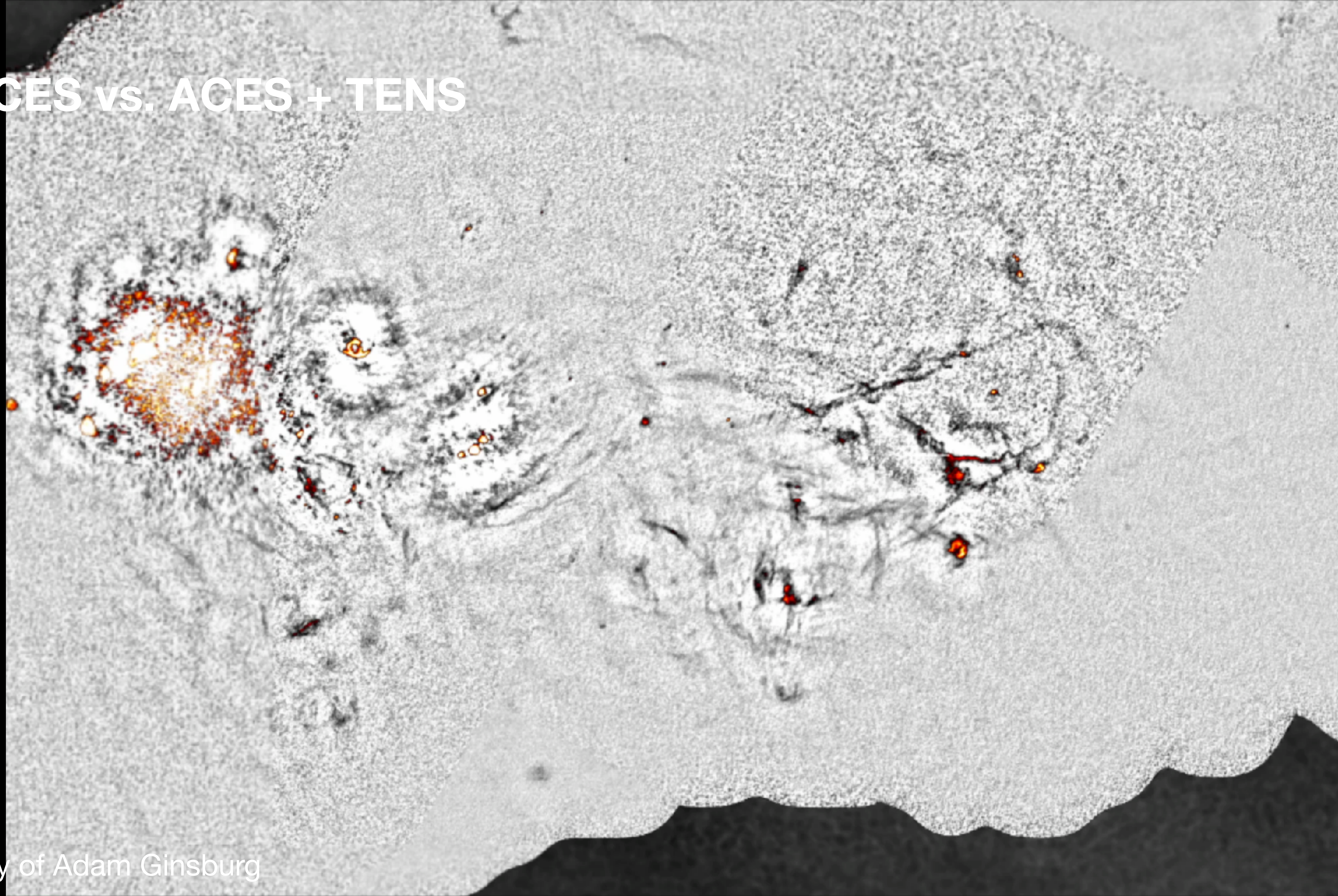


Radio continuum

MUSTANG-2 (+ Planck)

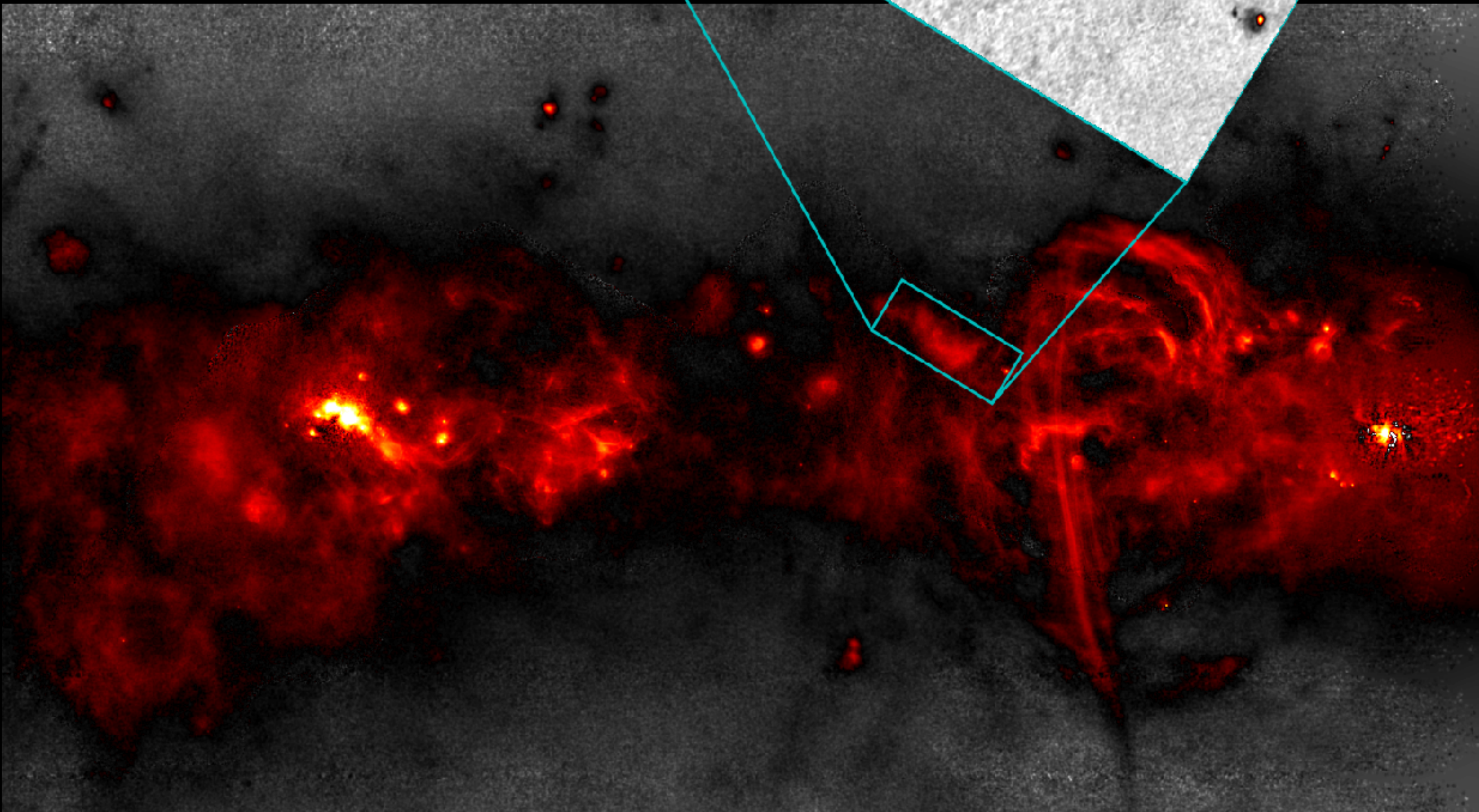


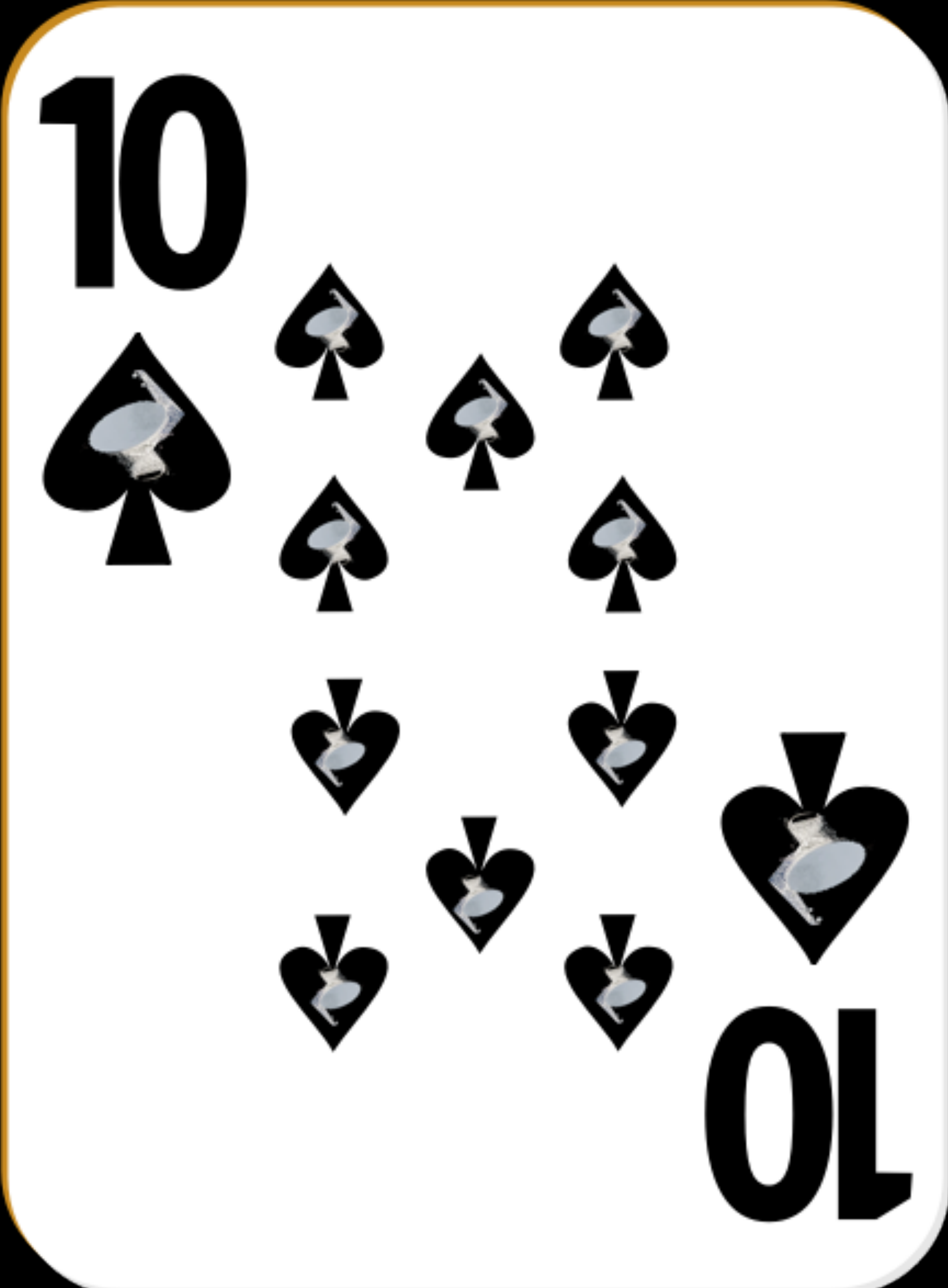
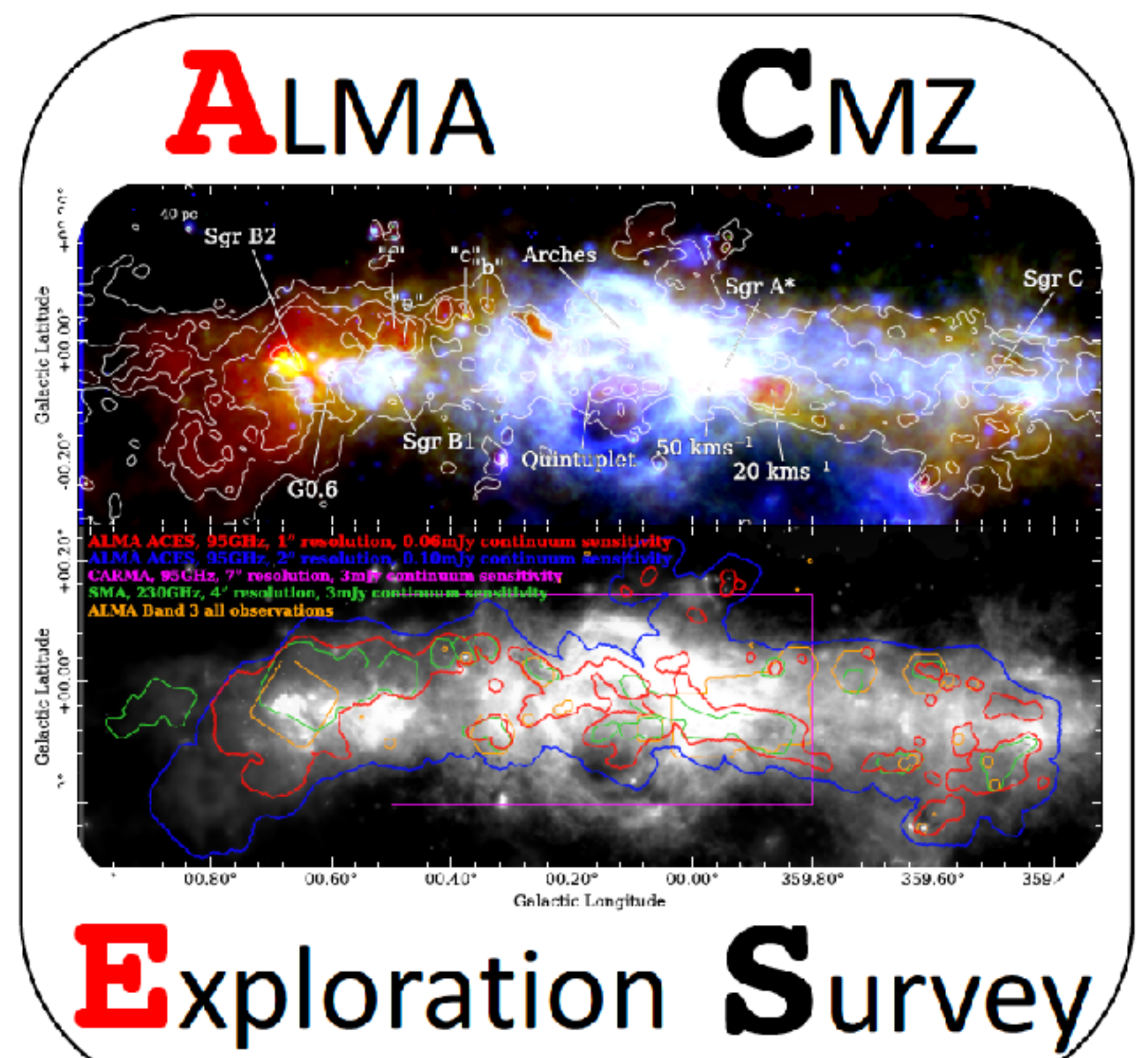
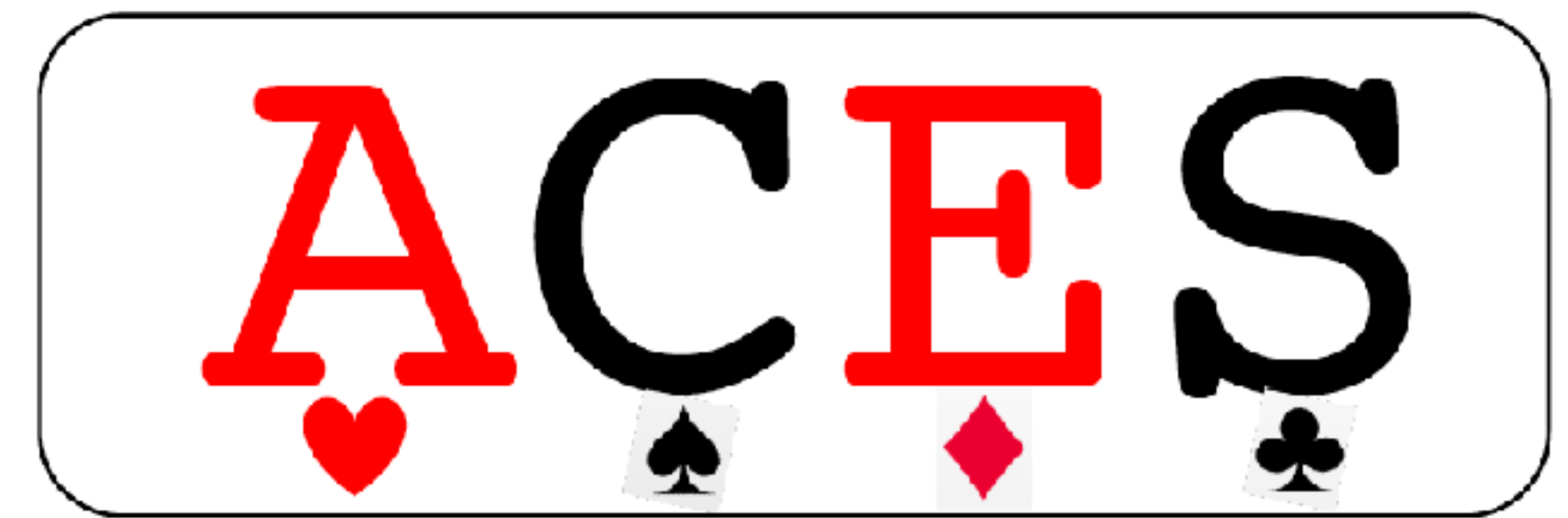
ACES vs. ACES + TENS

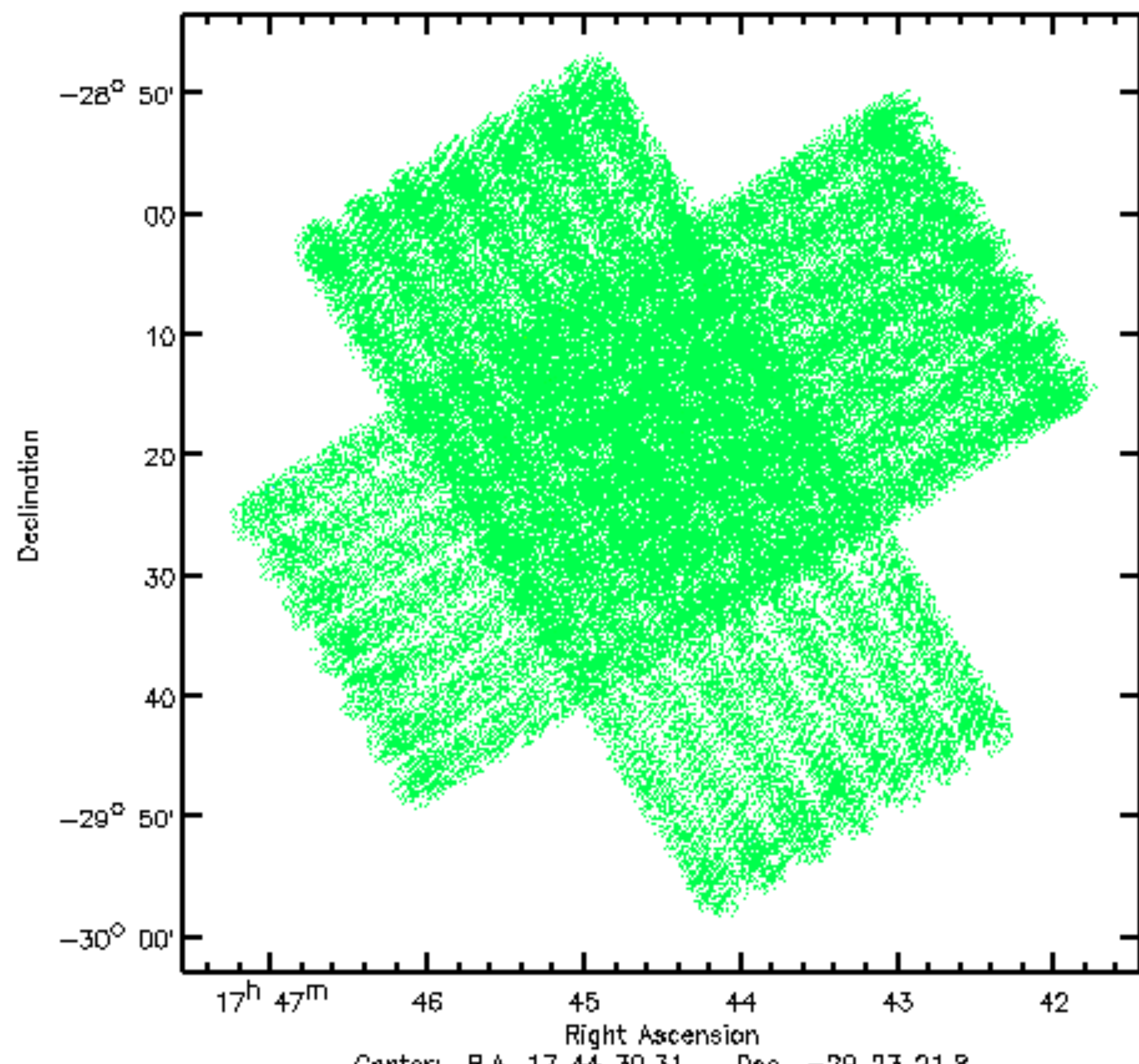
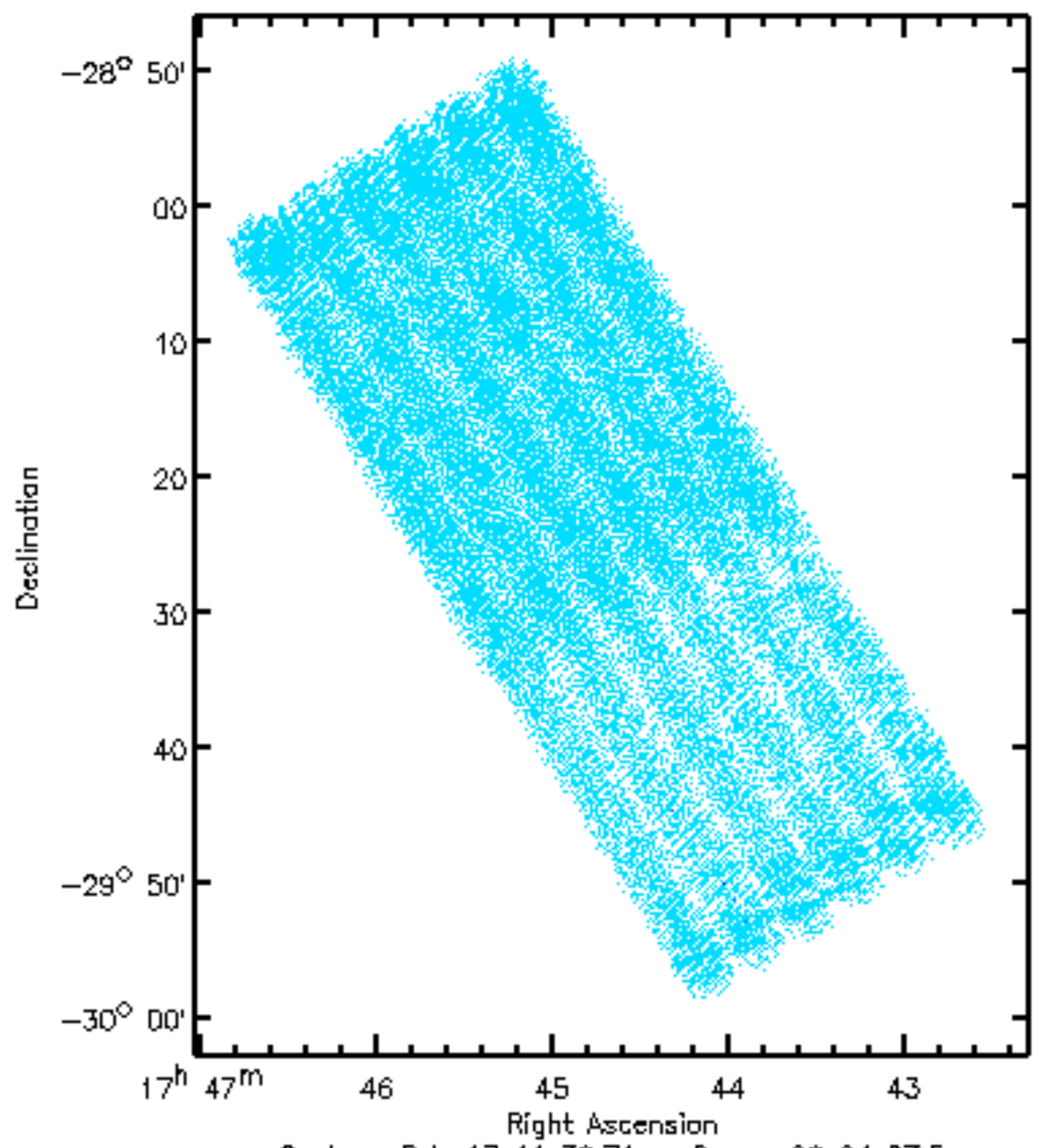


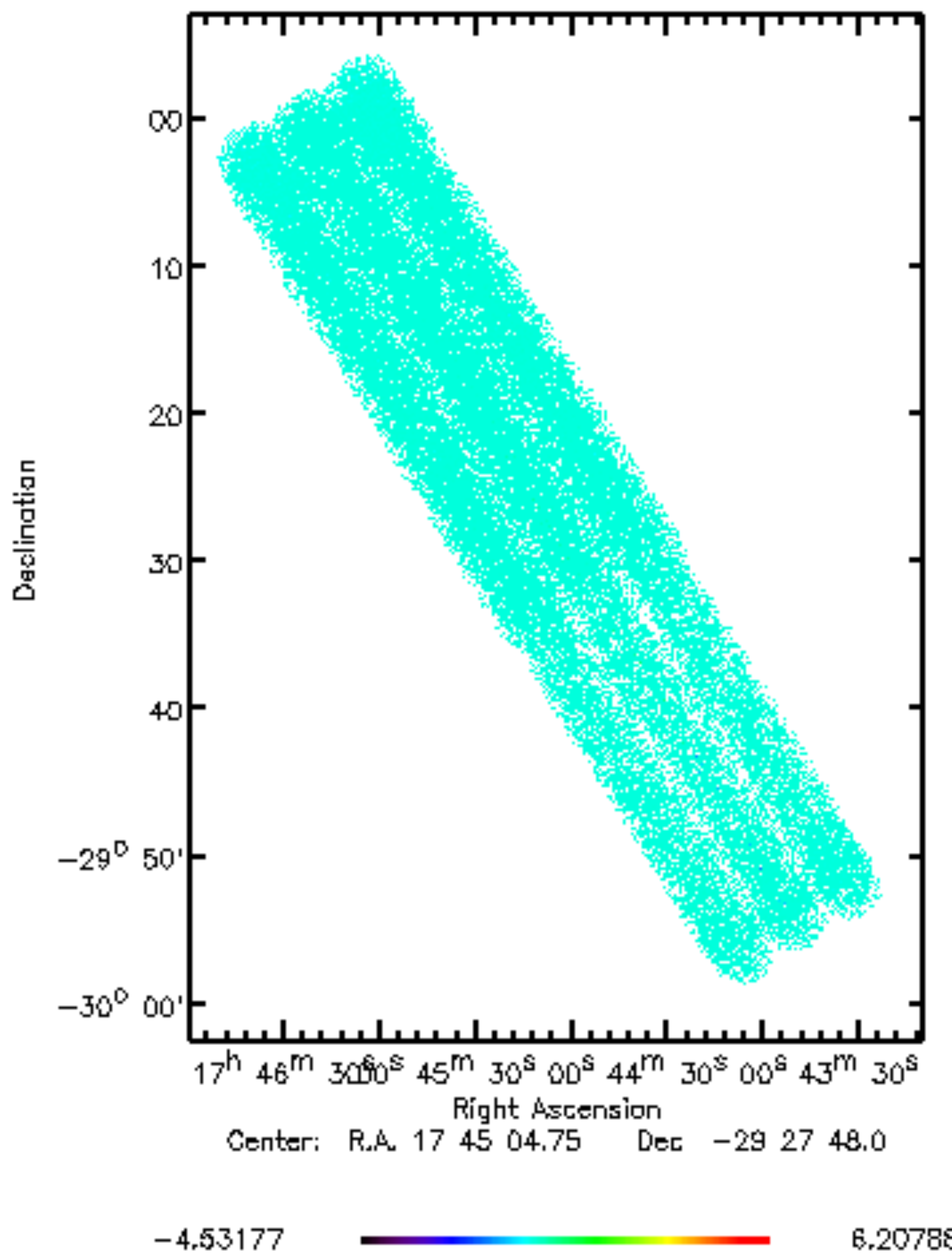
MUSTANG-2
+ ACES

ACES 12-m only









Thank you!

WLS

**Image credits appear next to images;
all uncredited images were either made
by me or are in the public domain.**



abulatek@ufl.edu



abulatek.github.io

Our "sister" station in Arizona stays on 550, and that market certainly does a job in the big, buying

KQY CBS PHOENIX, ARIZONA STILL AT 550

WE'RE MOVING TO 890

WLS "Moving Day," March 29th, (we go from 870 to 890) has been amply publicized, to insure no "listener loss" to advertisers—nor missed service to listeners.

Three full page, two-color advertisements in Prairie Farmer, totaling more than 1,020,000 circulation, largely in the WLS four-state, Major Coverage Area, have impressed the new location on Mid-West farm homes—and merchants. In addition, on several pages in the March 22 issue mention was made of the new WLS frequency.

For Chicago listeners a total of eight full-column ads in the Chicago Times have told the same story. A full page back cover ad in Radio Varieties spread the news farther, and every daily and weekly newspaper in the four-state area received

a news story, written from the WLS angle, but telling the full reallocation story.

15,000 cards explaining the change were distributed to visitors to the WLS National Barn Dance and studios. We supplied servicemen with WLS tabs for push button sets, to assure the station being represented on every radio.

WLS and Prairie Farmer are using stickers on all outgoing mail. And to complete the job of getting the story to everyone, we are using every possible moment on the air to announce the new frequency and explain the reasons for the change.

So, when WLS moves up to 890, we'll have our same full-size, loyal audience moving right along with us—for they all *know* that we're moving... why we're moving... and where, too!

50,000 WATTS NBC AFFILIATE

REPRESENTED BY JOHN BLAIR & COMPANY

The PRAIRIE FARMER STATION

BURRIDGE D. BUTLER President

GLENN SNYDER Manager

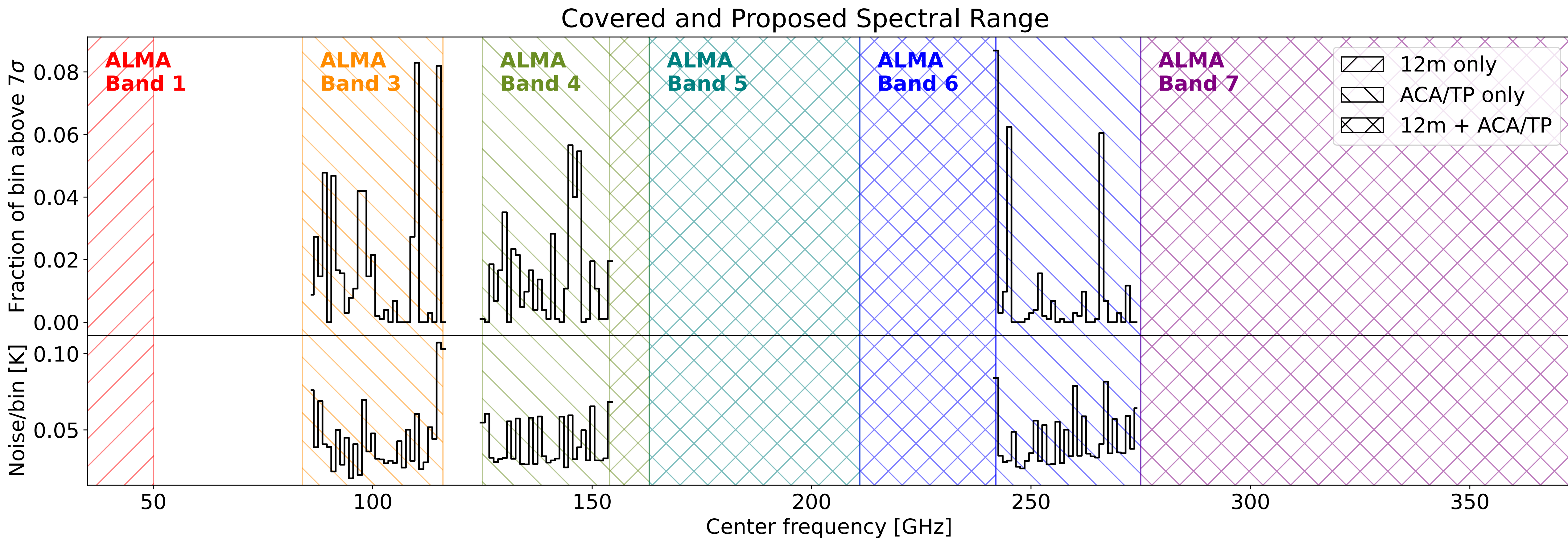
CHICAGO

Appendix

ALMA Cycle 11 Proposal

- Subm. in ALMA Cycles 8, 8S, 9, 10, 11

- See more lines of more molecules in missing bandwidth
- Cover larger angular scales with ACA/TP



Spectral Setup

ACES

